Looker, D. L. (1999). Acute and long-term stability studies of deoxy hemoglobin and characterization of ascorbate-induced modifications. *J. Pharm. Sci.* **88,** 79–88.

Klibanov, A. L., Maruyama, K., Torchilin, V. P., and Huang, L. (1990). Amphipathic polyethylene glycols effectively prolong the circulation time of liposomes. *FEBS Lett.* **268,** 235–237.

Li, S., Nickels, J., and Palmer, A. F. (2005). Liposome-encapsulated actin-hemoglobin (LEAcHb) artificial blood substitutes. *Biomaterials* **26,** 3759–3769.

Liu, L., and Yonetani, T. (1994). Preparation and characterization of liposome-encapsulated haemoglobin by a freeze–thaw method. *J. Microencapsul.* **11,** 409–421.

Loughrey, H. C., Bally, M. B., Reinish, L. W., and Cullis, P. R. (1990). The binding of phosphatidylglycerol liposomes to rat platelets is mediated by complement. *Thromb. Haemost.* **64,** 172–176.

Martini, J., Cabrales, P., Tsai, A. G., and Intaglietta, M. (2006). Mechanotransduction and the homeostatic significance of maintaining blood viscosity in hypotension, hypertension and haemorrhage. *J. Intern. Med.* **259,** 364–372.

Meyuhas, D., Nir, S., and Lichtenberg, D. (1996). Aggregation of phospholipid vesicles by water-soluble polymers. *Biophys. J.* **71,** 2602–2612.

Mobed, M., and Chang, T. M. S. (1991). Preparation and surface characterization of carboxymethylchitin-incorporated submicron bilayer-lipid membrane artificial cells (liposomes) encapsulating hemoglobin. *Biomater. Artif. Cells Immobilization Biotechnol.* **19,** 731–744.

Murray, J. A., Ledlow, A., Launspach, J., Evans, D., Loveday, M., and Conklin, J. L. (1995). The effects of recombinant human hemoglobin on esophageal motor function in humans. *Gastroenterology* **109,** 1241–1248.

Naito, Y., Fukutomi, I., Masada, Y., Sakai, H., Takeoka, S., Tsuchida, E., Abe, H., Hirayama, J., Ikebuchi, K., and Ikeda, H. (2002). Virus removal from hemoglobin solution using Planova membrane. *J. Artif. Organs* **5,** 141–145.

Natanson, C., Kern, S. J., Lurie, P., Banks, S. M., and Wolfe, S. M. (2008). Cell-free hemoglobin-based blood substitutes and risk of myocardial infarction and death: A meta-analysis. *JAMA* **299,** 2304–2312.

Ogata, Y., Goto, H., Kimura, T., and Fukui, H. (1997). Development of neo red cells (NRC) with the enzymatic reduction system of methemoglobin. *Artif. Cells Blood Substit. Immobil. Biotechnol.* **25,** 417–427.

Palmer, A. F., Sun, G., and Harris, D. R. (2009). Tangential flow filtration of hemoglobin. *Biotechnol. Prog.* **25,** 189–199.

Papahadjopoulos, D., Allen, T. M., Gabizon, A., Mayhew, E., Matthay, K., Huang, S. K., Lee, K. D., Woodle, M. C., Lasic, D. D., Redemann, C., and Martin, F. J. (1991). Sterically stabilized liposomes: Improvements in pharmacokinetics and antitumor therapeutic efficacy. *Proc. Natl. Acad. Sci. USA* **88,** 11460–11464.

Pape, A., Kertscho, H., Meier, J., Horn, O., Laout, M., Steche, M., Lossen, M., Theisen, A., Zwissler, B., and Habler, O. (2008). Improved short-term survival with polyethylene glycol modified hemoglobin liposomes in critical normovolemic anemia. *Intensive Care Med.* **34,** 1534–1543.

Phillips, W. T., Klipper, R., Fresne, D., Rudolph, A. S., Javors, M., and Goins, B. (1997). Platelet reactivity with liposome-encapsulated hemoglobin in the rat. *Exp. Hematol.* **25,** 1347–1356.

Phillips, W. T., Klipper, R. W., Awasthi, V. D., Rudolph, A. S., Cliff, R., Kwasiborski, V., and Goins, B. A. (1999). Polyethylene glycol-modified liposome-encapsulated hemoglobin: A long circulating red cell substitute. *J. Pharmacol. Exp. Ther.* **288,** 665–670.

Plock, J. A., Contaldo, C., Sakai, H., Tsuchida, E., Leunig, M., Banic, A., Menger, M. D., and Erni, D. (2005). Is the Hb in Hb vesicles infused for isovolemic hemodilution

necessary to improve oxygenation in critically ischemic hamster skin? *Am. J. Physiol. Heart Circ. Physiol.* **289,** H2624–H2631.

Plock, J. A., Tromp, A. E., Contaldo, C., Spanholtz, T., Sinovcic, D., Sakai, H., Tsuchida, E., Leunig, M., Banic, A., and Erni, D. (2007). Hemoglobin vesicles reduce hypoxia-related inflammation in critically ischemic hamster flap tissue. *Crit. Care Med.* **35,** 899–905.

Rabinovici, R., Rudolph, A. S., Ligler, F. S., Smith, E. F. 3rd, and Feuerstein, G. (1992). Biological responses to exchange transfusion with liposome-encapsulated hemoglobin. *Circ. Shock* **37,** 124–133.

Rabinovici, R., Rudolph, A. S., Vernick, J., and Feuerstein, G. (1993). A new salutary resuscitative fluid: Liposome encapsulated hemoglobin/hypertonic saline solution. *J. Trauma* **35,** 121–127.

Rudolph, A. S. (1988). The freeze–dried preservation of liposome encapsulated hemoglobin: A potential blood substitute. *Cryobiology* **25,** 277–284.

Rudolph, A. S., Klipper, R. W., Goins, B., and Phillips, W. T. (1991). *In vivo* biodistribution of a radiolabeled blood substitute: ^{99m}Tc-labeled liposome-encapsulated hemoglobin in an anesthetized rabbit. *Proc. Natl Acad. Sci. USA* **88,** 10976–10980.

Sakai, H., and Tsuchida, E. (2007). Hemoglobin-vesicles for a transfusion alternative and targeted oxygen delivery. *J. Liposome Res.* **17,** 227–235.

Sakai, H., Takeoka, S., Yokohama, H., Nishide, H., and Tsuchida, E. (1992). Encapsulation of Hb into unsaturated lipid vesicles and γ-ray polymerization. *Polym. Adv. Technol.* **3,** 389–394.

Sakai, H., Takeoka, S., Yokohama, H., Seino, Y., Nishide, H., and Tsuchida, E. (1993). Purification of concentrated Hb using organic solvent and heat treatment. *Protein Expr. Purif.* **4,** 563–569.

Sakai, H., Hamada, K., Takeoka, S., Nishide, H., and Tsuchida, E. (1996). Physical properties of hemoglobin vesicles as red cell substitutes. *Biotechnol. Prog.* **12,** 119–125.

Sakai, H., Takeoka, S., Park, S. I., Kose, T., Izumi, Y., Yoshizu, A., Nishide, H., Kobayashi, K., and Tsuchida, E. (1997). Surface-modification of hemoglobin vesicles with poly(ethylene glycol) and effects on aggregation, viscosity, and blood flow during 90%-exchange transfusion in anesthetized rats. *Bioconjug. Chem.* **8,** 23–30.

Sakai, H., Tsai, A. G., Kerger, H., Park, S. I., Takeoka, S., Nishide, H., Tsuchida, E., and Intaglietta, M. (1998). Subcutaneous microvascular responses to hemodilution with red cell substitutes consisting of polyethylene glycol-modified vesicles encapsulating hemoglobin. *J. Biomed. Mater. Res.* **40,** 66–78.

Sakai, H., Tsai, A. G., Rohlfs, R. J., Hara, H., Takeoka, S., Tsuchida, E., and Intaglietta, M. (1999). Microvascular responses to hemodilution with Hb-vesicles as red cell substitutes: Influences of O_2 affinity. *Am. J. Physiol. Heart Circ. Physiol.* **276,** H553–H562.

Sakai, H., Yuasa, M., Onuma, H., Takeoka, S., and Tsuchida, E. (2000a). Synthesis and physicochemical characterization of a series of hemoglobin-based oxygen carriers: Objective comparison between cellular and acellular types. *Bioconjug. Chem.* **11,** 56–64.

Sakai, H., Tomiyama, K., Sou, K., Takeoka, S., and Tsuchida, E. (2000b). Poly(ethylene glycol)-conjugation and deoxygenation enable long-term preservation of hemoglobin-vesicles as oxygen carriers in a liquid state. *Bioconjug. Chem.* **11,** 425–432.

Sakai, H., Hara, H., Yuasa, M., Tsai, A. G., Takeoka, S., Tsuchida, E., and Intaglietta, M. (2000c). Molecular dimensions of Hb-based O_2 carriers determine constriction of resistance arteries and hypertension. *Am. J. Physiol. Heart Circ. Physiol.* **279,** H908–H915.

Sakai, H., Horinouchi, H., Tomiyama, K., Ikeda, E., Takeoka, S., Kobayashi, K., and Tsuchida, E. (2001). Hemoglobin-vesicles as oxygen carriers: Influence on phagocytic activity and histopathological changes in reticuloendothelial system. *Am. J. Pathol.* **159,** 1079–1088.

Sakai, H., Takeoka, S., Wettstein, R., Tsai, A. G., Intaglietta, M., and Tsuchida, E. (2002a). Systemic and microvascular responses to the hemorrhagic shock and resuscitation with Hb-vesicles. *Am. J. Physiol. Heart Circ. Physiol.* **283,** H1191–H1199.

Sakai, H., Masada, Y., Takeoka, S., and Tsuchida, E. (2002b). Characteristics of bovine hemoglobin as a potential source of hemoglobin-vesicles for an artificial oxygen carrier. *J. Biochem.* **131,** 611–617.

Sakai, H., Horinouchi, H., Masada, Y., Yamamoto, M., Takeoka, S., Kobayashi, K., and Tsuchida, E. (2004a). Hemoglobin-vesicles suspended in recombinant human serum albumin for resuscitation from hemorrhagic shock in anesthetized rats. *Crit. Care Med.* **32,** 539–545.

Sakai, H., Masada, Y., Horinouchi, H., Ikeda, H., Takeoka, S., Suematsu, M., Kobayashi, K., and Tsuchida, E. (2004b). Physiologic capacity of reticuloendothelial system for degradation of hemoglobin-vesicles (artificial oxygen carriers) after massive intravenous doses by daily repeated infusions for 14 days. *J. Pharmacol. Exp. Ther.* **311,** 874–884.

Sakai, H., Masada, Y., Onuma, H., Takeoka, S., and Tsuchida, E. (2004c). Reduction of methemoglobin via electron transfer from photoreduced flavin: Restoration of O_2-binding of concentrated hemoglobin solution coencapsulated in phospholipid vesicles. *Bioconjug. Chem.* **15,** 1037–1045.

Sakai, H., Hisamoto, S., Fukutomi, I., Sou, K., Takeoka, S., and Tsuchida, E. (2004d). Detection of lipopolysaccharide in hemoglobin-vesicles by Limulus amebocyte lysate test with kinetic-turbidimetric gel clotting analysis and pretreatment of surfactant. *J. Pharm. Sci.* **93,** 310–321.

Sakai, H., Sato, A., Takeoka, S., and Tsuchida, E. (2007). Rheological property of hemoglobin vesicles (artificial oxygen carriers) suspended in a series of plasma substitute aqueous solutions. *Langmuir* **23,** 8121–8128.

Sakai, H., Sato, A., Masuda, K., Takeoka, S., and Tsuchida, E. (2008a). Encapsulation of concentrated hemoglobin solution in phospholipid vesicles retards the reaction with NO, but not CO, by intracellular diffusion barrier. *J. Biol. Chem.* **283,** 1508–1517.

Sakai, H., Sato, A., Sobolewski, P., Takeoka, S., Frangos, J. A., Kobayashi, K., Intaglietta, M., and Tsuchida, E. (2008b). NO and CO binding profiles of hemoglobin vesicles as artificial oxygen carriers. *Biochim. Biophys. Acta* **1784,** 1441–1447.

Sakai, H., Seishi, Y., Obata, Y., Takeoka, S., Horinouichi, H., Tsuchida, E., and Kobayashi, K. (2009a). Fluid resuscitation with artificial oxygen carriers in hemorrhaged rats: Profiles of hemoglobin-vesicle degradation and hematopoiesis for 14 days. *Shock* **31,** 192–200.

Sakai, H., Okamoto, M., Ikeda, E., Horinouchi, H., Kobayashi, K., and Tsuchida, E. (2009b). Histopathological changes of rat brain after direct injection of hemoglobin vesicles (oxygen carriers) and neurological impact in an intracerebral hemorrhage model. *J. Biomed. Mater. Res. A* **88A,** 34–42.

Sakai, H., Horinouchi, H., Tsuchida, E., and Kobayashi, K. (2009c). Hemoglobin-vesicles and red blood cells as carriers of carbon monoxide prior to oxygen for resuscitation after hemorrhagic shock in a rat model. *Shock* **31,** 507–514.

Sakai, H, Sato, A., Takeoka, S., and Tsuchida, E. (2009d). Mechanism of flocculate formation of phospholipid vesicles suspended in a series of water-soluble biopolymers. *Biomacromolecules* **10,** 2344–2350.

Sakai, H., Sato, A., Okuda, N., Takeoka, S., Maeda, N., and Tsuchida, E. (2009e). Peculiar flow patterns of RBCs suspended in viscous fluids and perfused through a narrow tube (25 μm). *Am. J. Physiol. Heart Circ. Physiol.* **297,** H905–H910.

Sato, T., Kobayashi, K., Sekiguchi, S., and Tsuchida, E. (1992). Characteristics of artificial red cells: Hemoglobin-encapsulated in poly-lipid vesicles. *ASAIO J.* **38,** M580–M584.

Sato, T., Sakai, H., Sou, K., Medebach, M., Glatter, O., and Tsuchida, E. (2009). Static structure and dynamics of hemoglobin vesicle (HbV) developed as a transfusion alternative. *J. Phys. Chem. B* **113,** 8418–8428.

Sheffield, C. L., Spates, G. E., Droleskey, R. E., Green, R., and DeLoach, J. R. (1987). Preparation of lipid-free human hemoglobin by dialysis and ultrafiltration. *Biotechnol. Appl. Biochem.* **9,** 230–238.

Sou, K., and Tsuchida, E. (2008). Electrostatic interactions and complement activation on the surface of phospholipid vesicle containing acidic lipids: Effect of the structure of acidic groups. *Biochim. Biophys. Acta* **1778,** 1035–1041.

Sou, K., Naito, Y., Endo, T., Takeoka, S., and Tsuchida, E. (2003). Effective encapsulation of proteins into size-controlled phospholipid vesicles using freeze–thawing and extrusion. *Biotechnol. Prog.* **19,** 1547–1552.

Sou, K., Klipper, R., Goins, B., Tsuchida, E., and Phillips, W. T. (2005). Circulation kinetics and organ distribution of Hb vesicles developed as a red blood cell substitute. *J. Pharmacol. Exp. Ther.* **312,** 702–709.

Szebeni, J., Breuer, J. H., Szelenyi, J. G., Bathori, G., Lelkes, G., and Hollan, S. R. (1984). Oxidation and denaturation of hemoglobin encapsulated in liposomes. *Biochim. Biophys. Acta* **798,** 60–67.

Szebeni, J., Di Iorio, E. E., Hauser, H., and Winterhalter, K. H. (1985). Encapsulation of hemoglobin in phospholipid liposomes: Characterization and stability. *Biochemistry* **24,** 2827–2832.

Szebeni, J., Fontana, J. L., Wassef, N. M., Mongan, P. D., Morse, D. S., Dobbins, D. E., Stahl, G. L., Bunger, R., and Alving, C. R. (1999). Hemodynamic changes induced by liposomes and liposome-encapsulated hemoglobin in pigs: A model for pseudoallergic cardiopulmonary reactions to liposomes. Role of complement and inhibition by soluble CR1 and anti-C5a antibody. *Circulation* **99,** 2302–2309.

Szebeni, J., Baranyi, L., Sávay, S., Bodó, M., Milosevits, J., Alving, C. R., and Bünger, R. (2005). Complement activation-related cardiac anaphylaxis in pigs: Role of C5a anaphylatoxin and adenosine in liposome-induced abnormalities in ECG and heart function. *Am. J. Physiol. Heart Circ. Physiol.* **290,** H1050–H1058.

Taguchi, K., Maruyama, T., Iwao, Y., Sakai, H., Kobayashi, K., Horinouchi, H., Tsuchida, E., Kai, T., and Otagiri, M. (2009a). Pharmacokinetics of single and repeated injection of hemoglobin-vesicles in hemorrhagic shock rat model. *J. Control. Release* **136,** 232–239.

Taguchi, K., Urata, Y., Anraku, M., Maruyama, T., Watanabe, H., Sakai, H., Horinouchi, H., Kobayashi, K., Tsuchida, E., Kai, T., and Otagiri, M. (2009b). Pharmacokinetic study of enclosed hemoglobin and outer lipid component after the administration of hemoglobin-vesicles as an artificial oxygen carrier. *Drug Dispos. Metabol.* **37,** 1456–1463.

Takahashi, A. (1995). Characterization of neo red cells (NRCs), their function and safety *in vivo* tests. *Artif. Cells Blood Substit. Immobil. Biotechnol.* **23,** 347–354.

Takeoka, S., Sakai, H., Nishide, H., and Tsuchida, E. (1993). Preparation conditions of human hemoglobin-vesicles covered with lipid membranes. *Jpn. J. Artif. Organs* **22,** 566–569.

Takeoka, S., Terase, K., Sakai, H., Yokohama, H., Nishide, H., and Tsuchida, E. (1994a). Interaction between phosphoslipid assemblies and hemoglobin (Hb). *J. Macromol. Sci. Pure Appl. Chem.* **A31,** 97–108.

Takeoka, S., Sakai, H., Terease, K., Nishide, H., and Tsuchida, E. (1994b). Characteristics of Hb-vesicles and encapsulation procedure. *Artif. Cells Blood Substit. Immobil. Biotechnol.* **22,** 861–866.

Takeoka, S., Ohgushi, T., Terase, K., and Tsuchida, E. (1996). Layer-controlled hemoglobin vesicles by interaction of hemoglobin with a phospholipid assembly. *Langmuir* **12,** 1755–1759.

Takeoka, S., Sakai, H., Kose, T., Mano, Y., Seino, Y., Nishide, H., and Tsuchida, E. (1997). Methemoglobin formation in hemoglobin vesicles and reduction by encapsulated thiols. *Bioconjug. Chem.* **8,** 539–544.

Takeoka, S., Teramura, Y., Atoji, T., and Tsuchida, E. (2002). Effect of Hb-encapsulation with vesicles on H_2O_2 reaction and lipid peroxidation. *Bioconjug. Chem.* **13,** 1302–1308.

Teramura, Y., Kanazawa, H., Sakai, H., Takeoka, S., and Tsuchida, E. (2003). The prolonged oxygen-carrying ability of Hb vesicles by coencapsulation of catalase *in vivo*. *Bioconjug. Chem.* **14,** 1171–1176.

Tsai, A. G., Friesenecker, B., McCarthy, M., Sakai, H., and Intaglietta, M. (1998). Plasma viscosity regulates capillary perfusion during extreme hemodilution in hamster skinfold model. *Am. J. Physiol. Heart Circ. Physiol.* **275,** H2170–H2180.

Tsuchida, E. Ed. (1998). *Blood Substitutes: Present and Future Perspectives*. Elsevier, Chichester.

Vandegriff, K. D., Young, M. A., Lohman, J., Bellelli, A., Samaja, M., Malavalli, A., and Winslow, R. M. (2008). CO-MP4, a polyethylene glycol-conjugated haemoglobin derivative and carbon monoxide carrier that reduces myocardial infarct size in rats. *Br. J. Pharmacol.* **154,** 1649–1661.

Vidal-Naquet, A., Gossage, J. L., Sullivan, T. P., Haynes, J. W., Gilruth, B. H., Beissinger, R. L., Sehgal, L. R., and Rosen, A. L. (1989). Liposome-encapsulated hemoglobin as an artificial red blood cell: Characterization and scale-up. *Biomater. Artif. Cells Artif. Organs* **17,** 531–552.

Vivier, A., Vuillemard, J. C., Ackermann, H. W., and Poncelet, D. (1992). Large-scale blood substitute production using a microfluidizer. *Biomater. Artif. Cells Immobilization Biotechnol.* **20,** 377–397.

Wakamoto, S., Fujihara, M., Abe, H., Sakai, H., Takeoka, S., Tsuchida, E., Ikeda, H., and Ikebuchi, K. (2001). Effects of poly(ethyleneglycol)-modified hemoglobin vesicles on agonist-induced platelet aggregation and RANTES release *in vitro*. *Artif. Cells Blood Substit. Immobil. Biotechnol.* **29,** 191–201.

Wakamoto, S., Fujihara, M., Abe, H., Yamaguchi, M., Azuma, H., Ikeda, H., Takeoka, S., and Tsuchida, E. (2005). Effects of hemoglobin vesicles on resting and agonist-stimulated human platelets *in vitro*. *Artif. Cells Blood Substit. Immobil. Biotechnol.* **33,** 101–111.

Wang, L., Morizawa, K., Tokuyama, S., Satoh, T., and Tsuchida, E. (1992). Modulation of oxygen-carrying capacity of artificial red cells (ARC). *Polym. Adv. Technol.* **4,** 8–11.

Winslow, R., and Chapman, K. W. (1994). Pilot-scale preparation of hemoglobin solutions. *Methods Enzymol.* **231,** 3–16.

Yamazaki, M., Aeba, R., Yozu, R., and Kobayashi, K. (2006). Use of hemoglobin vesicles during cardiopulmonary bypass priming prevents neurocognitive decline in rats. *Circulation* **114**(1 Suppl), I220–I225.

Yoshioka, H. (1991). Surface modification of haemoglobin-containing liposomes with poly (ethylene glycol) prevents liposome aggregation in blood plasma. *Biomaterials* **12,** 861–864.

Bone marrow-targeted liposomal carriers: a feasibility study in nonhuman primates

Background & aims: Recently, we described a novel surface-modified lipid vesicle formulation (liposome) that had very high targeting to bone marrow in normal rabbits. Because the bone marrow is the site of hematopoiesis, bone marrow-targeted drug-delivery systems have many potential applications. In this study we investigated whether these bone marrow-targeted vesicles are also similarly effective for bone marrow targeting in rhesus monkeys, a primate animal model that is more relevant to humans. **Materials & methods:** The preformed vesicles encapsulating 30 mM glutathione were labeled with technetium-99m (^{99m}Tc) for scintigraphic imaging. The vesicles were 216 ± 21 nm in diameter with a negative surface charge composed of DPPC, cholesterol, anionic amphiphile and poly(ethylene glycol)-DSPE (1:1:0.2:0.013 molar ratio). **Results:** The whole-body images of rhesus monkeys receiving intravenous ^{99m}Tc vesicles revealed high uptake of the ^{99m}Tc vesicles in bone marrow. Based on image analysis, we estimated that approximately 70% of the injected dose of the ^{99m}Tc vesicles was taken up by the bone marrow. **Conclusion:** This finding increases the feasibility of using this bone marrow-specific drug-delivery system for clinical applications.

KEYWORDS: biodistribution bone marrow drug carrier lipid vesicles liposomes nonhuman primate scintigraphy surface modification

Keitaro Sou[1,2]*, Beth Goins[3], Michelle M Leland[4], Eishun Tsuchida[1] & William T Phillips[3]

[1]Author for correspondence: Center for Advanced Biomedical Sciences, Waseda University (TWIns), Tokyo 162-8480, Japan. Tel.: +81 3 5273 2836; Fax: +81 3 3205 4740; k-sou@aurora.waseda.jp

[2]Research Institution for Science & Engineering, Waseda University, Tokyo 169-8555, Japan

[3]Department of Radiology, University of Texas Health Science Center at San Antonio, San Antonio, TX 78229-3900, USA

[4]Veterinarian-Laboratory Animal Resources, University of Texas Health Science Center at San Antonio, San Antonio, TX 78229-3900, USA

Phospholipid vesicles (liposomes) are one type of nanosized carrier for drug delivery [1–4]. Since the pharmacokinetics of liposomally encapsulated drugs are strongly dependent on the biodistribution of the liposomes, the tracking of the *in vivo* distribution of liposomes is an important factor in estimating the potential of a particular liposome formulation for specific drug-delivery applications. Whole-body radionuclide imaging is a powerful tool for noninvasive and quantitative determination of the biodistribution of liposomes in preclinical and clinical evaluations [5–7]. In particular, technetium-99m (^{99m}Tc), which has a photopeak of 140 keV and a half-life of 6 h, is a commonly used radionuclide for clinical scintigraphic imaging. To label liposomes encapsulating glutathione (GSH) with ^{99m}Tc, Phillips *et al.* has established a simple method using a complex of $^{99m}TcO_4$ and hexamethyl propyleneamine oxime (HMPAO) [8].

In general, whole-body scintigraphic imaging of animals and humans receiving conventional ^{99m}Tc liposomes demonstrates significant uptake of the ^{99m}Tc liposomes in the liver and spleen with minimal uptake in the bone marrow [6]. Significant phagocytic function of the mononuclear phagocyte system of the liver and spleen is a principal mechanism for capturing circulating vesicles *in vivo*. Tissue macrophages such as hepatic Kupffer cells and splenic macrophages are the cellular components responsible for the uptake of vesicles in these mononuclear phagocyte system organs [9]. To achieve a longer circulation of liposomes, their surface can be modified with poly(ethylene glycol) (PEG) chains, which function to decrease phagocytosis by macrophages in the liver and spleen [10–12].

On the other hand, phagocytes such as macrophages and dendritic cells are potential target cells for liposome-based drug delivery [13–17]. To specifically target liposomes to macrophages, known ligand molecules such as mannose have been attached to the surface of the liposomes. Recently, we found that rabbit bone marrow phagocytic cells selectively capture lipid vesicles that have been surface modified with an anionic amphiphile: L-glutamic acid, *N*-(3-carboxy-1-oxopropyl)-, 1,5-dihexadecyl ester (SA) [18]. This lipid, when added as a small fractional component of the liposome formulation, was serendipitously found to result in high uptake of the bone marrow in studies conducted for the development of an encapsulated blood substitute. Development of an effective bone marrow delivery system in humans could prove valuable owing to the vital importance of the bone marrow as the site of the crucial function of hematopoiesis. Bone marrow phagocytic cells are well known to provide important support to hematopoetic cells by serving as the

future medicine part of fsg

central component of erythroblastic islands [19]. Potential clinical uses of this bone marrow-delivery system include delivery of agents that protect the marrow from the toxic effects of chemotherapy and radiation, and the delivery of agents to effectively and safely ablate bone marrow prior to bone-marrow transplant. The present study was carried out to determine if vesicles that are surface modified with SA and PEG (PEG-[SA-Ve]) can effectively target bone marrow in a primate. For this purpose, we examined the biodistribution of PEG-[SA-Ve] in rhesus monkeys by noninvasive scintigraphic imaging.

Materials & methods

Materials

1,2-dipalmitoyl-*sn*-glycero-3-phosphocholine (DPPC), cholesterol and SA were purchased from Nippon Fine Chemical Co. Ltd. (Osaka, Japan). SA was custom synthesized based on previous reports [20]. 1,2-distearoyl-*sn*-glycero-3-phosphoethanolamine-*N*-[monomethoxy PEG (5000)] (PEG-DSPE) was purchased from NOF Co. (Tokyo, Japan). GSH was purchased from Sigma (St Louis, MO, USA).

Preparation of vesicles

Mixed lipid powder of DPPC, cholesterol, SA and PEG-DSPE (1:1:0.2:0.013 molar ratio) was hydrated with phosphate-buffered saline (pH 6.0) containing 30 mM GSH at 5 gdl^{-1}. After controlling vesicle size by an extrusion method (final pore size of the filter: 0.2 µm, Isopore™, Millipore, Tokyo, Japan), the unencapsulated GSH was removed by two ultracentrifugation steps (3×10^5 g, 60 min each) and PEG-[SA-Ve] encapsulating GSH were dispersed in phosphate-buffered saline at 6.2 gdl^{-1}. The diameter of the final PEG-[SA-Ve] determined by dynamic light scattering was 216 ± 21 nm.

^{99m}Tc-labeling of PEG-[SA-Ve]

Radiolabeling of preformed vesicles was performed according to a method described previously [7,18]. A saline solution of sodium (^{99m}Tc) pertechnetate (5 ml, 2.78 GBq [75 mCi]; GE Healthcare Radiopharmacy, San Antonio, TX, USA) was injected into a vial containing lyophilized HMPAO (0.5 mg, $SnCl_2$; 7.6 mg; Ceretec™; GE Healthcare, Arlington, IL, USA). The mixed solution was incubated for 5 min at room temperature. The ^{99m}Tc-HMPAO solution (0.6 ml) was then added to PEG-[SA-Ve] dispersion ([lipids] = 6.2 gdl^{-1}, 0.6 ml), and the resulting mixture was incubated for 1 h. After removing free ^{99m}Tc-HMPAO by gel filtration (Sephadex-G25 column), total radioactivity was measured in a dose calibrator (AtomLab 100, Biodex, Shirley, NY, USA) and the labeling efficiency was calculated as the percentage of radioactivity in ^{99m}Tc-PEG-[SA-Ve] after separation to radioactivity measured just before gel-filtration chromatography.

Animal experiments

The animal experiments were performed under the NIH Animal Use and Care guidelines and approved by the University of Texas Health Science Center at San Antonio Institutional Animal Care and Use Committee (TX, USA). The male rhesus monkeys (11.2–15.0 kg; n = 3) were sedated with ketamine 10 mg/kg intramuscularly. They were maintained sedated with 2% isoflurane gas anesthesia and placed in the supine position under a Picker (Cleveland, OH, USA) large-field-of-view γ-camera interfaced with a Pinnacle imaging computer (Medasys, Ann Arbor, MI, USA). ^{99m}Tc-PEG-[SA-Ve] (total lipid dose: 15 mg/kg bodyweight; ^{99m}Tc activity, 237–337 MBq [6.4–9.1 mCi]) were injected in the venous line of the animals at 1 ml min^{-1}. The 1 -min dynamic 128 × 128 pixel anterior scintigraphic images were acquired over a continuous period of 1 h. Then static images were acquired at 1, 3 and 22 h after injection of ^{99m}Tc-PEG-[SA-Ve]. Blood samples (100 µl) were collected into tubes at various times post-injection to monitor circulation persistence. The radioactivity of the blood samples was counted in an automated scintillation well counter (Wallac 1480, Perkin Elmer Life Sciences, Boston, MA, USA). The counts at each time point were normalized to the percentage of the counts in the first blood sample collected immediately after ^{99m}Tc-PEG-[SA-Ve] injection.

Image analysis

Region of interest analysis was performed by drawing regions of interest for all the regions of the body demonstrating uptake on the images. These regions included the liver, spleen and the bone marrow uptake regions including the skull, neck vertebrae, right and left clavicles, right and left upper limbs, the ribs, sternum, upper spine, lower spine, pelvis, sacrum and right and left lower limbs. Total count activity in all regions was considered to be 100% of the injected dose of activity. The percentage of activity in the whole body was then calculated for each region by dividing by the total body counts and multiplying by 100. This analysis was performed at 3 and 22 h and the results are shown in Table 1.

Since dynamic images were acquired at 1-min intervals for the first 1 h, dynamic region of interest activity as a percentage of activity following the complete infusion of the dose of 10 min was calculated as the percentage change in the particular region from the baseline 10-min image. The results from this analysis are shown in FIGURE 1.

Results

Preparation of ^{99m}Tc-PEG-[SA-Ve]

The lipid membrane of present PEG-[SA-Ve] is composed of four different lipids, as shown in FIGURE 2. In addition to DPPC and cholesterol, which are common components of most conventional liposome formulations, the vesicles contain an anionic amphiphile (SA) and PEG-lipid (PEG-DSPE). The average diameter of PEG-[SA-Ve] was controlled to 216 ± 21 nm by the stepwise extrusion through membrane filters with a final pore size of 0.2 µm. Preformed PEG-[SA-Ve] encapsulating GSH was labeled with ^{99m}Tc to allow investigation of PEG-[SA-Ve] biodistribution quantitatively. The ^{99m}Tc labeling of the vesicles encapsulating GSH was accomplished by using a complex of the ^{99m}Tc and HMPAO. Stoichiometric analysis has shown a 2:1 molar ratio of GSH and ^{99m}Tc for stable complex formation [21]. The ^{99m}Tc-labeling efficiencies were reproducible with the three individual runs of 81, 86 and 82%. We have confirmed that 98% of the incorporated ^{99m}Tc remains with present vesicle formulation after incubation in plasma at 37°C for 24 h [18]. This high encapsulation stability supports the accuracy of the ^{99m}Tc-PEG-[SA-Ve] biodistribution results.

Circulation & biodistribution kinetics

^{99m}Tc-PEG-[SA-Ve] was intravenously injected into anesthetized rhesus monkeys (n = 3) at 15 mg lipids/kg bodyweight. The circulation half-life times of ^{99m}Tc-PEG-[SA-Ve] in each monkey were 1.3, 2.8 and 4.0 h. The averaged profile of the ^{99m}Tc-PEG-[SA-Ve] elimination from blood circulation is shown in FIGURE 3. At 22 h postinjection, the ^{99m}Tc-PEG-[SA-Ve] have almost disappeared from circulation (<3% of injected ^{99m}Tc-PEG-[SA-Ve] in blood). As shown in FIGURE 1A, the γ-camera images show intense radioactivity in blood pool of the heart and liver at 10 min after injection of ^{99m}Tc-PEG-[SA-Ve]. At 60 min, the radioactivity of heart clearly is decreased owing to the elimination of ^{99m}Tc-PEG-[SA-Ve] from the blood circulation. On the other hand, liver still had strong radioactivity at 60 min. The radioactivity of bone marrow in the shoulder, sternum and spine is increased with time, indicating the distribution of the ^{99m}Tc-PEG-[SA-Ve] to these organs from the blood circulation. The percentage of radioactivity at each time point to that at 10 min postinjection showed that the ^{99m}Tc-PEG-[SA-Ve] gradually distributed to the shoulder, lower spine and liver with time (FIGURE 1B). In particular, the increase of radioactivity in the shoulder bone marrow was remarkable.

Table 1. Estimated biodistribution of ^{99m}Tc-PEG-[SA-Ve] in rhesus monkeys at 3 and 22 h (n = 2).

Numbered regions‡		% of ^{99m}Tc- PEG-[SA-Ve]	
		3 h	*22 h*
L, S	L and S	28.0	27.2
1	Skull	8.3	6.7
2	Neck vertebrae	2.2	2.4
3	Right clavicle	0.7	0.5
4	Left clavicle	0.6	0.6
5	Right upper limb (shoulder and arm)	4.5	5.4
6	Left upper limb (shoulder and arm)	4.7	5.8
7	Ribs, sternum and upper spine	21.0	21.3
8	Lower spine	11.3	14.7
9	Lower limbs (pelvis, sacrum, tail, femur and tibia)	19.0	15.7
Total bone marrow uptake		72.0	72.9

*These biodistribution percentages are estimated based on region of interest counts uncorrected for ^{99m}Tc-PEG-[SA-Ve] activity in circulating blood. Circulating blood activity is contributing to a portion of the activity at 3 h, but very little at 22 h when virtually all activity has been cleared from the circulation.

‡These correspond to the numbered regions in the γ-camera image of FIGURES 4 & 5.

^{99m}Tc: Technetium-99m; L: Liver; PEG: Poly(ethylene glycol); S: Spleen; SA: L-glutamic acid, N-(3-carboxy-1-oxopropyl)-, 1,5-dihexadecyl ester.

Whole-body imaging

The whole-body γ-camera images were acquired at 1, 3 and 22 h after injection of ^{99m}Tc-PEG-[SA-Ve]. All three monkeys showed significant distribution of ^{99m}Tc-PEG-[SA-Ve] in bone marrow but one monkey was removed from the whole-body image analysis because it was incidentally discovered to have a liver mass. Biodistribution images of two monkeys are shown in FIGURES 4 & 5. The high overall uptake of ^{99m}Tc-PEG-[SA-Ve] throughout the bone marrow is easily visualized at 3 and 22 h in two different monkeys. The skull, sternum, shoulders, spine and pelvis were especially active to ^{99m}Tc-PEG-[SA-Ve] uptake in monkeys. From the image analysis, we estimated that approximately 70% of ^{99m}Tc-PEG-[SA-Ve] is distributed into the bone marrow, as summarized in TABLE 1. The other 30% was distributed in the liver and spleen. These results clearly indicate that the bone marrow is a principal organ of PEG-[SA-Ve] uptake in rhesus monkey.

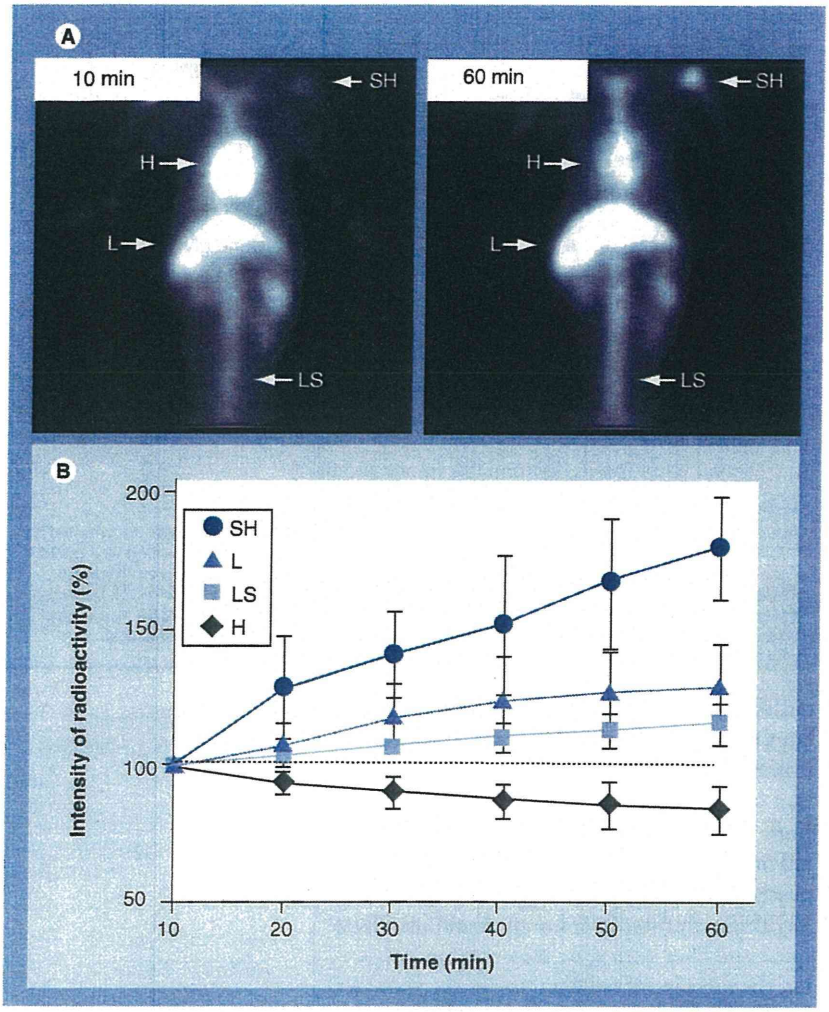

Figure 1. Initial distribution kinetics of ^{99m}Tc-PEG-[SA-Ve] after intravenous injection (lipids: 15 mg/kg bodyweight) in rhesus monkeys. (A) γ-camera images of a rhesus monkey acquired at 10 and 60 min postinjection of ^{99m}Tc-PEG-[SA-Ve]. **(B)** Intensity profile of radioactivity at the region of interest with time. The intensity of radioactivity at each time point was expressed as a percentage of the radioactivity at 10 min postinjection. The uptake is shown to increase in the bone marrow over the first 60 min of the study during which time the activity is clearing in the heart, which correlates with the clearance of the ^{99m}Tc-PEG-[SA-Ve] from the blood circulation.
^{99m}Tc: Technetium-99m; H: Heart; L: Liver; LS: Lower spine; PEG: Poly(ethylene glycol); SA: L-glutamic acid, *N*-(3-carboxy-1-oxopropyl)-, 1,5-dihexadecyl ester; SH: Shoulder.

Discussion

The present study focused on PEG-[SA-Ve], which are composed of lipids modified with SA and PEG. In a previous study, we have identified that the SA is an active factor leading to their phagocytosis by bone marrow macrophages in rabbits [18]. The specific mechanism of why SA lipid is associated with high bone marrow macrophage uptake is not known; however, its uptake is likely owing to interaction with scavenger receptors on the bone marrow macrophages that are important in the removal of senescent blood cells and also in the phagocytosis of extruded erythroblast nuclei [22,23]. As little as 0.6 mol% of PEG-DSPE can depress hepatic uptake without depressing bone marrow uptake. The active targeting factor of SA and the passive targeting factor of PEG-DSPE appear to cooperatively increase the distribution of vesicles to bone marrow. However, the species specificity of bone marrow macrophages for uptake of PEG-[SA-Ve] was unclear. Therefore, the present experiments in a primate are important for future translational research and clinical applications.

After injection of PEG-[SA-Ve] in rhesus monkeys, they were eliminated from the blood circulation with a half-life of several hours, as shown in Figure 3. Based on previous studies in rabbits, the highest percentage uptake in the bone marrow was found with a lipid dose of 15 mg lipid/kg bodyweight [18,24]. Based on these prior studies in rabbits, we selected this dose of 15 mg lipid/kg bodyweight for the present study.

One significant finding offered by the present study is that PEG-[SA-Ve] are promising carriers for delivering encapsulated agents to primate bone marrow. The whole-body images impressively show that the primate bone marrow has significant phagocytic activity for these specially modified circulating particles, as shown in Figures 4 & 5. In particular, the skull, sternum, shoulders, spine and pelvis demonstrated uptake of PEG-[SA-Ve] in all monkeys tested. The injected doses of ^{99m}Tc-PEG-[SA-Ve] in the liver, spleen and bone marrow were calculated from the distribution of radioactivity in these three organs. This image analysis revealed that approximately 70% of the injected dose of ^{99m}Tc-PEG-[SA-Ve] were distributed in the bone marrow. This ^{99m}Tc-PEG-[SA-Ve] uptake by bone marrow is nearly identical to the level determined from a previous experiment in rabbits (> 60% of injected dose ^{99m}Tc-PEG-[SA-Ve]). However, in contrast to the distribution of PEG-[SA-Ve] in bone marrow throughout the whole body in rabbits, there was less ^{99m}Tc-PEG-[SA-Ve] distributed in the legs and arms of the monkeys. In adult humans, the myeloid hematopoiesis is distributed in red marrow, which is mainly localized in the ribs, sternum, spine, pelvis and proximal shafts of the femora and humeri [25]. It seems that the distribution of PEG-[SA-Ve] in monkeys is similar to the distribution of myeloid hematopoiesis in humans. The scintigraphic imaging of PEG-[SA-Ve] distribution appears to show the location of hematopoietic activity in bone marrow, which may be useful for the diagnosis of hematopoietic disorders.

In a recent study [Sou K, Goins B, Oyajobi BO, Travi BL, Phillips WT, Manuscript in Preparation], PEG-[SA-Ve] did not show a very high uptake in the bone marrow of rats, while they had a much higher uptake in the spleen of rats than in the spleen of rabbits and primates. The reason for this species difference in bone marrow distribution is unknown. We believe this difference may be related to the relatively larger spleen-to-bodyweight ratios found in rats as compared with rabbits and primates. We also believe this species difference may be due to the much higher cell production and turnover in the spleen of rats relative to the bone marrow as compared with rabbits and primates, which likely have higher cell production and turnover in the bone marrow. Extramedullary hematopoeisis has been shown to commonly occur in the spleen of rats while being much less common in rabbits and primates [26]. The significant differences in bone-marrow uptake between the rats and rabbits/rhesus monkeys demonstrates the importance of studying nanoparticle distributions in a variety of animal species, particular larger animals such as rabbits and primates. Quantitative noninvasive imaging studies of the distribution of nanoparticles in larger animals can best be done with scintigraphic imaging.

The distribution of the ^{99m}Tc-PEG-[SA-Ve] in rhesus monkeys found in this study is very different from a previous imaging study of a standard liposome formulation in rhesus monkeys as reported by Dams *et al.* [27]. In the Dams *et al.* study, ^{99m}Tc-liposomes which were composed of partially hydrogenated egg-phosphatidylcholine, cholesterol and PEG (Mw. 2000)-DSPE showed significant liver and spleen uptake but no significant bone marrow uptake of the ^{99m}Tc-liposomes. This demonstrates that conventional liposomes are not taken up by the bone marrow of rhesus monkeys and suggests that bone-marrow uptake of PEG-[SA-Ve] is specifically related to its lipid formulation. This bone-marrow specificity appears to provide a mechanism for site-specific drug delivery to the bone marrow from the blood circulation. Thus, the present PEG-[SA-Ve] system is regarded as a successful example of *in vivo* site-specific targeting by specific surface modification of liposomes. The specific participation of bone marrow macrophages in the clearance of circulating particles such as lipoproteins and neutrophils has been shown previously [28–30]. Interestingly, the uptake of apoptotic neutrophils by bone marrow macrophages was shown to stimulate the production of granulocyte-colony stimulating factor [29]. Furthermore, bone marrow macrophages, associated with erythroblasts in a hematopoietic environment, participate in erythropoiesis control and engulfment of nuclei from erythroid precursor

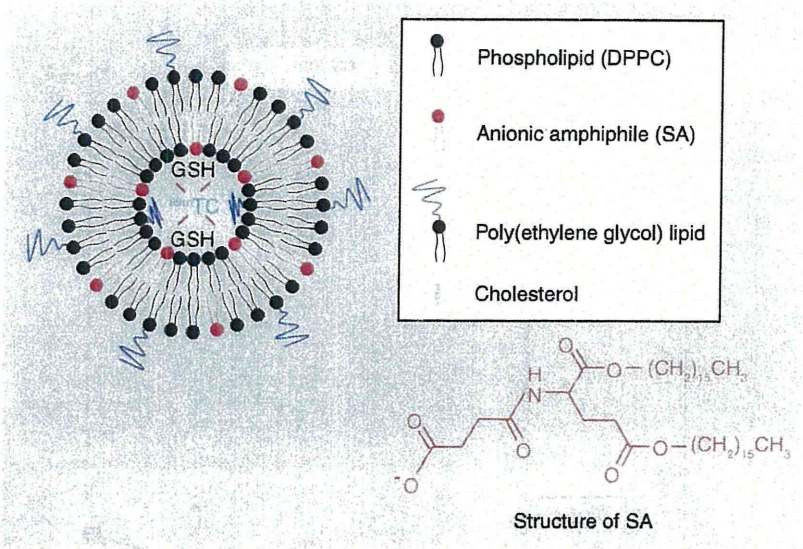

Figure 2. Bone marrow-targeted liposomal carriers (PEG-[SA-Ve]) labeled with ^{99m}Tc. The lipid bilayer membrane is composed of four lipids and the surface is specialized by an anionic amphiphile (SA) with succinic acid moiety and a poly(ethylene glycol) lipid. ^{99m}Tc is remotely loaded into preformed vesicles encapsulating 30 mM GSH.
^{99m}Tc: Technetium-99m; DPPC: 1,2-dipalmitoyl-*sn*-glycero-3-phosphocholine; GSH: Glutathione; PEG: Poly(ethylene glycol); SA: L-glutamic acid, *N*-(3-carboxy-1-oxopropyl)-, 1,5-dihexadecyl ester.

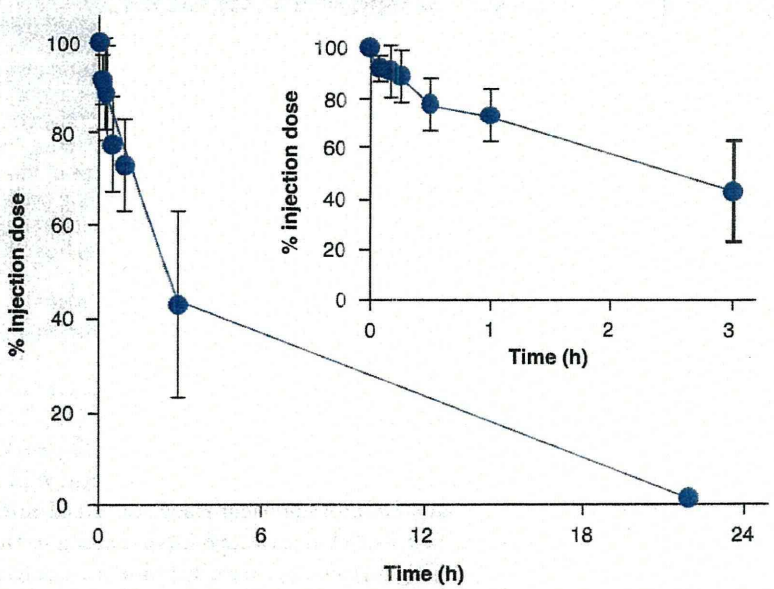

Figure 3. Circulation kinetics of ^{99m}Tc-PEG-[SA-Ve] after intravenous injection (lipids: 15 mg/kg) in rhesus monkeys. The percentage of radioactivity is calculated as a percentage of the baseline radioactivity in a blood sample withdrawn just after injection.
^{99m}Tc: Technetium-99m; PEG: Poly(ethylene glycol); SA: L-glutamic acid, *N*-(3-carboxy-1-oxopropyl)-, 1,5-dihexadecyl ester.

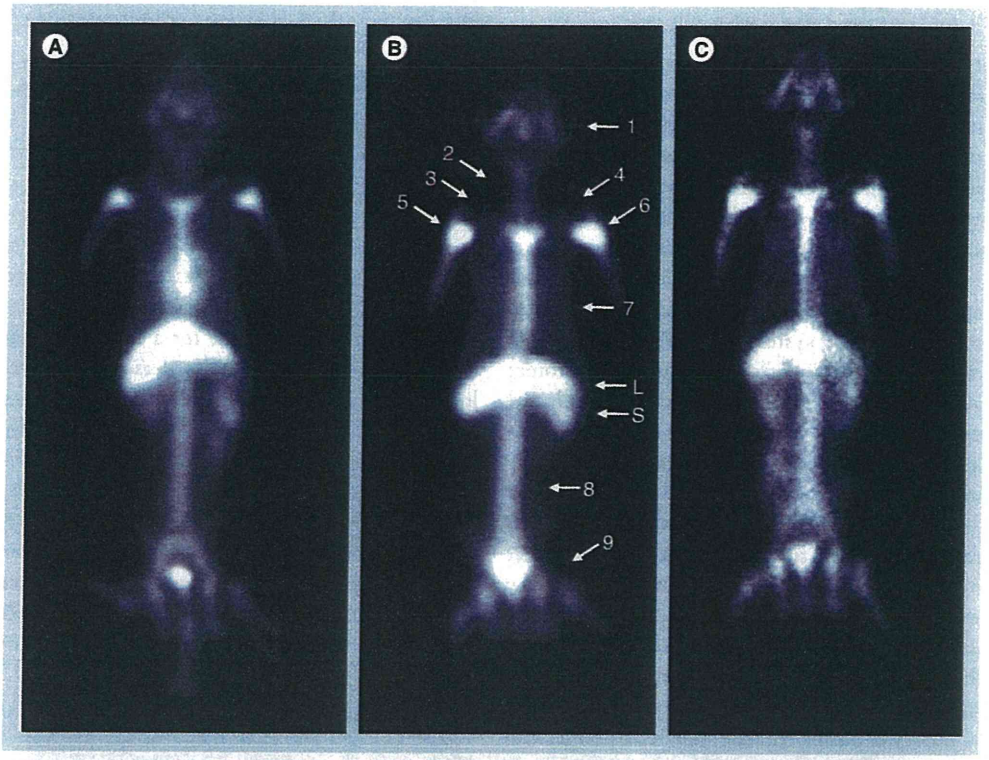

Figure 4. Static γ-camera images of rhesus monkey number 1 at (A) 1, (B) 3 and (C) 22 h postinjection of ^{99m}Tc-PEG-[SA-Ve]. Numbered regions are 1: skull; 2: neck; 3: right clavicle; 4: left clavicle; 5: right upper limbs (shoulder and arm); 6: left upper limbs (shoulder and arm); 7: ribs, sternum and upper spine; 8: lower spine; 9: lower limbs (pelvis, sacrum, tail, femur and tibia). ^{99m}Tc: Technetium-99m; L: Liver; PEG: Poly(ethylene glycol); S: Spleen; SA: L-glutamic acid, *N*-(3-carboxy-1-oxopropyl)-, 1,5-dihexadecyl ester.

cells [19,22,31]. Such specific biology of bone marrow macrophages in controlling hematopoiesis may offer a therapeutic avenue for PEG-[SA-Ve] to deliver the therapeutic agents directly to bone marrow macrophages.

In a prior study by Senior and Gregoriadis, 35% of the injected dose of intravenously administered small unilamellar liposomes composed of DSPC and cholesterol (1:1) and encapsulating ^{111}In-bleomycin as a tracer with a size of 65 nm accumulated in the carcass/bone of mice and rats at 72 h [32]. In this article, it was presumed that the liposomes were taken up by the phagocytic cells of the bone marrow. This previous study describes a high uptake of liposomes in the bone marrow of rats, whereas the bone marrow-targeted liposomes in the present study do not have high bone-marrow uptake in rats [Sou K, Goins B, Oyajobi BO, Travi BL, Phillips WT, Manuscript in Preparation] but do have high bone-marrow uptake in rabbits [18] and in the rhesus monkey primate model. It is also possible that the high apparent uptake in the Senior and Gregoriadis study may be due to the postmetabolism distribution of ^{111}In, as 90% of the tracer had cleared from the blood by 24 h, but the tissue biodistribution was not performed until 72 h. High bone-marrow uptake has not been shown in subsequent studies with liposomes of this formulation labeled with other radiotracers.

To the best of our knowledge, this is the first carrier system that has been described that can specifically deliver a very high quantity of intravenously injected therapeutic agents to bone marrow in a primate model. There are many potential applications of this delivery system [33,34]; however, the success of these applications will depend on the nature of the drug being delivered and its interaction with bone marrow macrophages, which are the likely cells of uptake in the marrow. For some applications, the drug may need to be released from the phagolysosome of the bone marrow macrophage to reach its therapeutic target located within the macrophage cytoplasm. In other applications, there may need to be a complete release of the liposome-encapsulated drug from the bone marrow macrophage so that the drug can move to other cells located in the bone marrow that contain the therapeutic target. Previous studies have shown

that macrophages in culture that have phagocytosed liposome-encapsulated doxorubicin can release the majority of the doxorubicin intact into the cell media, providing clear evidence that macrophage-ingested drugs can be completely released [35]. Other studies have also shown that macrophages can be loaded with drugs to serve as cellular drug-delivery vehicles [36,37].

Assuming the drug targeting and release issues can be overcome, potential uses of this bone-marrow delivery system include: the delivery of chemo- and radio-protective agents to protect sensitive bone marrow during radiation and chemotherapy treatments; the delivery of agents to specifically ablate bone marrow prior to bone marrow transplant; the delivery of gene therapy to bone marrow; the specific delivery of antimicrobial agents to treat parasitic diseases that reside in high concentrations in bone marrow macrophages such as leishmania; and the delivery of diagnostic agents to the bone marrow to assess bone-marrow mass and provide precise localization of bone marrow. In patients receiving radiation treatment, knowledge of the size and location of the marrow in a particular patient is important for accurate quantification of radiation dose to bone marrow, which is the organ most sensitive to radiation and chemotherapy toxicity.

Another potential application of PEG-[SA-Ve] in cancer is the delivery of anticancer drugs into bone marrow. This bone marrow-specific drug-delivery system may allow for a more targeted therapy of hematopoietic disorders such as myeloleukemia and myeloma. Furthermore, recent evidence indicates that macrophages can be targeted as a method to suppress angiogenesis in solid tumors [14,38,39]. In addition, PEG-[SA-Ve] encapsulating a macrophage-depleting agent such as clodronate may be able to selectively deplete the bone marrow macrophages. On the other hand, myelosuppression is a frequent side effect of cancer chemotherapy and radiotherapy. In this

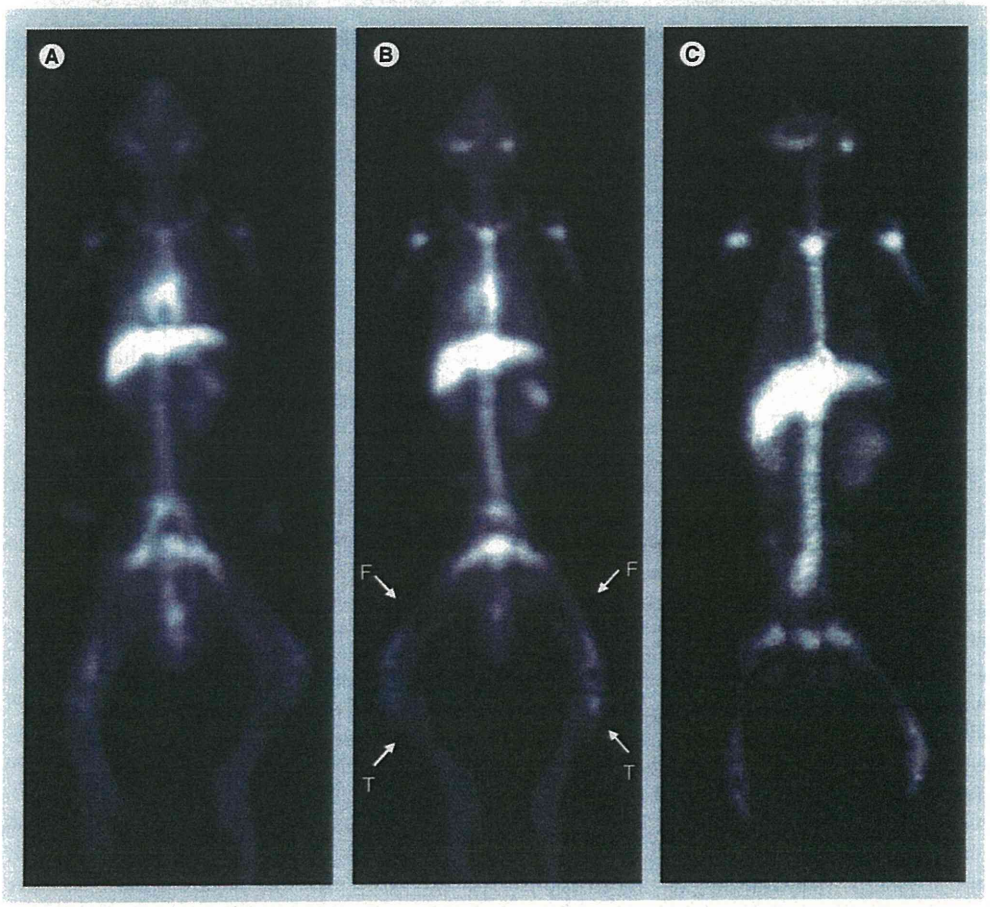

Figure 5. Static γ-camera images of rhesus monkey number 2 at (A) 1, (B) 3 and (C) 22 h postinjection of ^{99m}Tc-PEG-[SA-Ve]. In this second monkey, uptake in the proximal tibia was more prominent.
^{99m}Tc: Technetium-99m; F: Femur; PEG: Poly(ethylene glycol); SA: L-glutamic acid, *N*-(3-carboxy-1-oxopropyl)-, 1,5-dihexadecyl ester; T: Tibia.

instance, PEG-[SA-Ve] may be used as a vehicle to deliver protective agents to bone marrow with the goal of reducing myelosuppression.

Conclusion

The clear demonstration of bone marrow targeting of the SA surface-modified vesicles in the rhesus monkey model, in addition to the previous demonstration of bone marrow targeting in rabbits, suggests that the mechanism of uptake relies upon a common mechanism likely to be present in a large number of large mammals. More importantly, it is likely that human subjects will have a similar pattern of increased bone marrow uptake of these vesicles, opening the possibility for development of bone marrow-specific nanomedicines.

Future perspective

This bone marrow-specific drug-delivery system may facilitate targeted therapy of many therapeutic agents. Further research will need to be performed to demonstrate the feasibility of this carrier system for these different therapeutic applications.

Financial & competing interests disclosure

This work was partly supported by the Japan Society for the Promotion of Science (JSPS) Bilateral Joint Project between Japan-US. The authors have no other relevant affiliations or financial involvement with any organization or entity with a financial interest in or financial conflict with the subject matter or materials discussed in the manuscript apart from those disclosed.

No writing assistance was utilized in the production of this manuscript.

Ethical conduct of research

The authors state that they have obtained appropriate institutional review board approval or have followed the principles outlined in the Declaration of Helsinki for all human or animal experimental investigations. In addition, for investigations involving human subjects, informed consent has been obtained from the participants involved.

Executive summary

- Bone marrow is the principal site of uptake of the present PEG-[SA-Ve] formulation in rhesus monkeys, a primate closely related to humans genetically.
- Whole-body region of interest scintigraphic image analysis of monkeys receiving intravenous ^{99m}Tc-PEG-[SA-Ve] revealed that approximately 70% of the injected dose was taken up by the bone marrow.
- This bone marrow-specific drug-delivery system may facilitate targeted therapy of agents to protect the bone marrow, as well as agents to specifically ablate the bone marrow prior to bone-marrow transplant. It may also provide an effective delivery system for gene therapy and the specific treatment of hematopoietic malignancies.

Bibliography

1 Bangham AD, Horne RW: Negative staining of phospholipids and their structure modification by surface-active agents as observed in the electron microscope. *J. Mol. Biol.* 8, 660–668 (1964).

2 Papahadjopoulos D, Allen TM, Gabizon A *et al.*: Sterically stabilized liposomes: improvements in pharmacokinetics and antitumor therapeutic efficacy. *Proc. Natl Acad. Sci. USA* 88, 11460–11464 (1991).

3 Torchilin VP: Recent advances with liposomes as pharmaceutical carriers. *Nat. Rev. Drug Discov.* 4, 145–160 (2005).

4 Sofuo S: Surface-active liposomes for targeted cancer therapy. *Nanomed.* 2, 711–724 (2007).

5 Goins B, Phillips WT: The use of scintigraphic imaging as a tool in the development of liposome formulations. *Prog. Lipid Res.* 40, 95–123 (2001).

6 Laverman P, Brouwers AH, Dams ET *et al.*: Preclinical and clinical evidence for disappearance of long-circulating characteristics of polyethylene glycol liposomes at low lipid dose. *J. Pharmacol. Exp. Ther.* 293, 996–1001 (2000).

7 Phillips WT, Goins BA, Bao A: Radioactive liposomes. *Wiley Interdiscip. Rev. Nanomed. Nanobiotechnol.* 1, 69–83 (2009).

8 Phillips WT, Rudolph AS, Goins B, Timmons JH, Klipper R, Blumhardt R: A simple method for producing a technetium-99m labeled liposome which is stable *in vivo*. *Nucl. Med. Biol.* 19, 539–547(1992).

9 Moghimi SM, Hunter AC, Murray JC: Long-circulating and target-specific nanoparticles: theory to practice. *Pharmacol. Rev.* 53, 283–318 (2001).

10 Klibanov AL, Maruyama K, Torchilin VP, Huang L: Amphipatic poly(ethylene glycol)s effectively prolong the circulation time of liposome. *FEBS Lett.* 268, 235–237 (1990).

11 Woodle MC, Lasic DD: Sterically stabilized liposome. *Biochim. Biophys. Acta* 1113, 171–199 (1992).

12 Phillips WT, Klipper RW, Awasthi VD *et al.*: Polyethylene glycol-modified liposome-encapsulated hemoglobin: a long circulating red cell substitute. *J. Pharmacol. Exp. Ther.* 288, 665–670 (1999).

13 Chellat F, Merhi Y, Moreau A, Yahia L'H: Therapeutic potential of nanoparticulate systems for macrophage targeting. *Biomaterials* 26, 7260–7275 (2005).

14 Zeisberger SM, Odermatt B, Marty C, Zehnder-Fjällman AHM, Ballmer-Hofer K, Schwendener RA: Clodronate-liposome-mediated depletion of tumour-associated macrophages: a new and highly effective antiangiogenic therapy approach. *Br. J. Cancer* 95, 272–281 (2006).

15 Sou K, Inenaga S, Takeoka S, Tsuchida E: Loading of curcumin into macrophages using lipid-based nanoparticles. *Int. J. Pharm.* 352, 287–293 (2008).

16 Wijagkanalan W, Kawakami S, Takenaga M, Igarashi R, Yamashita F, Hashida M: Efficient targeting to alveolar macrophages by intratracheal administration of mannosylated liposomes in rats. *J. Control. Release* 125, 121–130 (2008).

17 Espuelas S, Thumann C, Heurtault B, Schuber F, Frisch B: Influence of ligand valency on the targeting of immature human dendritic cells by mannosylated liposomes. *Bioconjug. Chem.* 19, 2385–2393 (2008).

18 Sou K, Goins B, Takeoka S, Tsuchida E, Phillips WT: Selective uptake of surface-modified phospholipid vesicles by bone marrow macrophages *in vivo*. *Biomaterials* 28, 2655–2666 (2007).

19 Chasis JA, Mohandas N: Erythroblastic islands: niches for erythropoiesis. *Blood* 112, 470–478 (2008).

20 Sou K, Naito Y, Endo T, Takeoka S, Tsuchida E: Effective encapsulation of proteins into size-controlled phospholipid vesicles using freeze-thawing and extrusion. *Biotechnol. Prog.* 19, 1547–1552 (2003).

21 Baba K, Moretti JL, Weinmann P, Senekowitsch-Schmidtke R, Ercan MT: Tc-glutathione complex (Tc-GSH): labelling, chemical characterization and biodistribution in rats. *Met. Based Drugs* 6, 329–336 (1999).

22 Yoshida H, Kawane K, Koike M, Mori Y, Uchiyama Y, Nagata S: Phosphatidylserine-dependent engulfment by macrophages of nuclei from erythroid precursor cells. *Nature* 437, 754–758 (2005).

23 Fadeel B, Quinn P, Xue D, Kagan V: Fat(al) attraction: oxidized lipids act as 'eat-me' signals. *HFSP J.* 1, 225–229 (2007).

24 Sou K, Klipper R, Goins B, Tsuchida E, Phillips WT: Circulation kinetics and organ distribution of Hb-vesicles developed as a red blood cell substitute. *J. Pharmacol. Exp. Ther.* 312, 702–709 (2005).

25 Morrie E, Kricun MD: Red–yellow marrow conversion: its effect on the location of some solitary bone lesions. *Skeletal Radiol.* 14, 10–19 (1985).

26 Woodburn KW, Wilson SD, Fong KL, Schatz PJ, Spainhour CB, Norton D: Chronic pharmacological and safety evaluation of Hematide, a PEGylated peptidic erythropoiesis-stimulating agent, in rodents. *Basic Clin. Pharmacol. Toxicol.* 104, 155–163 (2009).

27 Dams ET, Laverman P, Oyen WJ *et al.*: Accelerated blood clearance and altered biodistribution of repeated injections of sterically stabilized liposomes. *J. Pharmacol. Exp. Ther.* 292, 1071–1079 (2000).

28 Hussain MM, Mahley RW, Boyles JK, Lindquist PA, Brecht WJ, Innerarity TL: Chylomicron metabolism. Chylomicron uptake by bone marrow in different animal species. *J. Biol. Chem.* 264, 17931–17938 (1989).

29 Furze RC, Rankin SM: The role of the bone marrow in neutrophil clearance under homeostatic conditions in the mouse. *FASEB J.* 22, 3111–3119 (2008).

30 Furze RC, Rankin SM: Neutrophil mobilization and clearance in the bone marrow. *Immunology* 125, 281–288 (2008).

31 Sadahira Y, Mori M: Role of the macrophage in erythropoiesis. *Pathol. Int.* 49, 841–848. (1999).

32 Senior J, Crawley JC, Gregoriadis G: Tissue distribution of liposomes exhibiting long half-lives in the circulation after intravenous injection. *Biochim. Biophys. Acta* 839, 1–8 (1985).

33 Szabó R, Peiser L, Plüddenmann A *et al.*: Uptake of branched polypeptides with poly[L-Lys] backbone by bone-marrow culture-derived murine macrophages: the role of the class A scavenger receptor. *Bioconjug. Chem.* 16, 1442–1450 (2005).

34 Moghimi SM: Exploiting bone marrow microvascular structure for drug delivery and future therapies. *Adv. Drug Deliv. Rev.* 17, 61–73 (1995).

35 Storm G, Steerenberg PA, Emmen F, van Borssum Waalkes M, Crommelin DJ: Release of doxorubicin from peritoneal macrophages exposed *in vivo* to doxorubicin-containing liposomes. *Biochim. Biophys. Acta* 965, 136–145 (1988).

36 Burke B, Sumner S, Maitland N, Lewis CE: Macrophages in gene therapy: cellular delivery vehicles and *in vivo* targets. *J. Leukoc. Biol.* 72, 417–28 (2002).

37 Ikehara Y, Niwa T, Biao L *et al.*: A carbohydrate recognition-based drug delivery and controlled release system using intraperitoneal macrophages as a cellular vehicle. *Cancer Res.* 66, 8740–8748 (2006).

38 Sunderkötter C, Steinbrink K, Goebeler M, Bhardwaj R, Sorg C: Macrophages and angiogenesis. *J. Leukoc. Biol.* 55, 410–422 (1994).

39 Hiraoka K, Zenmyo M, Watari K *et al.*: Inhibition of bone and muscle metastases of lung cancer cells by a decrease in the number of monocytes/macrophages. *Cancer Sci.* 99, 1595–1602 (2008).

Am J Physiol Heart Circ Physiol 298: H956–H965, 2010.
First published December 31, 2009; doi:10.1152/ajpheart.00741.2009.

Hemoglobin encapsulation in vesicles retards NO and CO binding and O_2 release when perfused through narrow gas-permeable tubes

Hiromi Sakai,[1,2] Naoto Okuda,[3] Atsushi Sato,[3] Tatsuya Yamaue,[4] Shinji Takeoka,[2,3] and Eishun Tsuchida[1]

[1]*Research Institute for Science and Engineering, Waseda University, Tokyo, Japan;* [2]*Waseda Bioscience Research Institute in Singapore, Republic of Singapore;* [3]*Graduate School of Advanced Sciences and Engineering, Waseda University, Tokyo, Japan; and* [4]*Kobelco Research Institute, Inc., Kobe, Japan*

Submitted 10 August 2009; accepted in final form 29 December 2009

Sakai H, Okuda N, Sato A, Yamaue T, Takeoka S, Tsuchida E. Hemoglobin encapsulation in vesicles retards NO and CO binding and O_2 release when perfused through narrow gas-permeable tubes. *Am J Physiol Heart Circ Physiol* 298: H956–H965, 2010. First published December 31, 2009; doi:10.1152/ajpheart.00741.2009.—Intravenous administration of cell-free Hb induces vasoconstriction and circulatory disorders, presumably because of the intrinsic affinities to endogenous nitric oxide (NO) and carbon monoxide (CO) as vasorelaxation factors and because of the facilitated O_2 release that might induce autoregulatory vasoconstriction. We examined these gas reactions when Hb-containing solutions of four kinds were perfused through artificial narrow tubes at a practical Hb concentration (10 g/dl). Purified Hb solution, polymerized bovine Hb ($Poly_BHb$), encapsulated Hb [Hb-vesicles (HbV), 279 nm], and red blood cells (RBCs) were perfused through a gas-permeable narrow tube (25 μm inner diameter) at 1 mm/s centerline velocity. The level of reactions was determined microscopically based on the visible-light absorption spectrum of Hb. When the tube was immersed in NO and CO atmospheres, both NO binding and CO binding of deoxygenated Hb (deoxy-Hb) and $Poly_BHb$ in the tube was faster than those of HbV and RBCs, and HbV and RBCs showed almost identical binding rates. When the tube was immersed in a N_2 atmosphere, oxygenated Hb and $Poly_BHb$ showed much faster O_2 release than did HbV and RBCs. $Poly_BHb$ showed a faster reaction than Hb because of the lower O_2 affinity of $Poly_BHb$ than Hb. The diffusion process of the particles was simulated using Navier-Stokes and Maxwell-Stefan equations. Results clarified that small Hb (6 nm) diffuses laterally and mixes rapidly. However, the large-dimension HbV shows no such rapid diffusion. The purely physicochemical differences in diffusivity of the particles and the resulting reactivity with gas molecules are one factor inducing biological vasoconstriction of Hb-based oxygen carriers.

microcirculation; blood substitutes; gas biology; liposome; erythrocytes

CELL-FREE, HEMOGLOBIN-BASED oxygen carriers (HBOCs) have been developed for use as transfusion alternatives. Some examples are intramolecular cross-linked Hb, polymerized Hb, and polyethylene glycol conjugated Hbs (5). The realization of HBOCs has long been anticipated, because they are free of pathogens and blood-type antigens and are storable for a long time for using at emergency situations. Some are in the final stage of clinical trials (23). The major remaining hurdle before clinical approval of this earliest generation of HBOCs is vasoconstriction and resulting hypertension, which are presumably attributable to the high reactivity of Hb with endothelium-derived nitric oxide (NO) (26, 28, 55). It has been suggested that small molecular Hbs permeate across the endothelial cell layer to the space near by the smooth muscle and inactivate NO. However, cellular Hb-vesicles (HbV) that encapsulate concentrated Hb solution in phospholipid vesicles (37) induce neither vasoconstriction nor hypertension (32). A physicochemical analysis using stopped-flow rapid scan spectrophotometry clarified that Hb encapsulation in vesicles retards NO binding compared with molecular Hb, because an intracellular diffusion barrier of NO is formed. The requisites for this diffusion barrier are *1*) a more concentrated intracellular Hb solution, and *2*) a larger particle size (34, 36). Even though various kinds of liposome-encapsulated Hb have been studied by many groups (29, 38), our HbV encapsulates a highly concentrated Hb solution (>35 g/dl) with a regulated large-particle diameter (250–280 nm) and attains 10 g/dl Hb concentration in the suspension. The absence of vasoconstriction in the case of intravenous HbV injection might be related to the lowered NO-binding rate constant, although it is much larger than that of red blood cells (RBCs) (34), and the lowered permeability across the endothelial cell layer in the vascular wall.

The proposed mechanism of vasoconstriction induced by HBOCs in relation to gaseous molecules is not limited to NO scavenging (31, 46, 50). For example, endogenous carbon monoxide (CO) is produced by constitutive hemeoxygenase-2 in hepatocytes; it serves as a vasorelaxation factor in hepatic microcirculation. Small molecular Hb permeates across the fenestrated endothelium, scavenges CO, and induces constriction of sinusoids and augments peripheral resistance (8). Oversupply of O_2 induces autoregulatory vasoconstriction to regulate the O_2 supply (10, 14, 16, 19). Injection of small HBOCs induces vasoconstriction, probably because of the facilitated O_2 transport (1, 18).

These reports imply the importance of studying the reaction profiles of HBOCs with NO, CO, and O_2. Stopped flow-rapid scan spectrophotometry and flash photolysis are common methods to define the binding and dissociation rate constants of Hb (25, 26, 31, 34, 36, 42). However, the Hb concentration in a cuvette must be diluted extremely, e.g., to 2 μM heme concentration ([Hb] = 0.003 g/dl), which is much lower than the practical concentration of HBOC injections ([Hb] = 4–13 g/dl). Moreover, the results of flash photolysis depend on the quantum yield (Φ = 0.5 for CO; 0.002 for NO) (43). This is not practical for larger particles, such as HbV, because the photodissociated gas molecule would remain in the particles before the rebinding profiles are observed (11). The results do not necessarily reflect the in vivo physiological circulatory condition, especially in small arteries and arterioles, so-called resistance vessels, where blood flow is strictly regulated. We are interested in the reaction profiles of HBOC fluids of a practical concentration without considering any biological effect, such as permeation across the endothelial cell layer in the vascular wall.

Address for reprint requests and other correspondence: H. Sakai, Associate Professor and Principal Investigator, Waseda Bioscience Research Institute in Singapore, 11 Biopolis Way, #05-01/02 Helios, 138667 Republic of Singapore (e-mail: hiromi@waseda.jp).

Gas-permeable narrow tubes enable the measurement of the O_2-releasing rates of HBOCs and RBCs during their flow through the tubes at a practical [Hb] (6–13 g/dl) (18, 27, 40, 48). As described in this paper, we used gas-permeable narrow tubes made of perfluorinated polymer to study not only O_2 release, but also NO-binding and CO-binding profiles, all of which should relate to the mechanisms of vasoactive properties of cell-free HBOCs and the vasoinactive properties of cellular HbV proposed above.

MATERIALS AND METHODS

Preparations of HbV, Stroma-free Hb, Polymerized Hb, and Human RBCs

HbV was prepared as reported previously (33, 40, 45, 47), with slight modifications. Human Hb solution was obtained through purification of outdated RBCs provided by the Japanese Red Cross Society (Tokyo, Japan). Then Hb was stabilized by carbonylation (HbCO) and concentrated by ultrafiltration to 38 g/dl. Subsequently, pyridoxal 5′-phosphate (PLP; Sigma, St. Louis, MO) was added to the HbCO solution as an allosteric effector at a molar ratio of PLP/Hb tetramer = 2.5. We use PLP instead of 2,3-diphosphoglyceric acid, because 2,3-diphosphoglyceric acid is chemically unstable (53). The Hb solution with PLP was then mixed with lipids and encapsulated in vesicles. The lipid bilayer comprised 1,2-dipalmitoyl-*sn*-glycero-3-phosphatidylcholine, cholesterol, 1,5-*O*-dihexadecyl-*N*-succinyl-L-glutamate (Nippon Fine Chemical, Osaka, Japan), and 1,2-distearoyl-*sn*-glycerol-3-phosphatidylethanolamine-*N*-PEG_{5000} (NOF, Tokyo, Japan) at a molar composition of 5:5:1:0.033. The particle diameter was regulated using the extrusion method (45). The encapsulated HbCO was converted to oxyhemoglobin (HbO_2) by exposing the liquid membrane of HbV to visible light under an O_2 atmosphere. Finally, the Hb concentration of the suspension was adjusted to 10 g/dl. The particle size distribution was measured using a light-scattering method (Submicron Particle Size Analyzer, model N4 PLUS; Beckman Coulter, Fullerton, CA).

Purified human Hb solution suspended in phosphate-buffered saline (PBS) solution was prepared and mixed with PLP at molar ratios of PLP/Hb tetramer = 4 ([Hb] = 10 g/dl). We also used polymerized bovine Hb ($_B$Hb) solution ($Poly_BHb$) designed for veterinary use (oxyglobin; Biopure, Cambridge, MA) (2, 3), which is a mixture of nonpolymerized tetrameric $_B$Hb (37.2%) and $Poly_BHb$ with a broad molecular weight distribution. The $Poly_BHb$ solution (13 g/dl) was diluted to 10 g/dl using PBS. $Poly_BHb$ was only one chemically modified Hb that was commercially available, and its physicochemical properties and the presence of vasoconstrictive effect were documented (2, 3). We used this product as the standard product as a negative control.

For this study, we used fresh human blood specimens. The study was approved by Waseda University's Ethics Committee on Medical Research Involving Human Subjects and performed according to the World Medical Association Declaration of Helsinki and Title 45, US Code of Federal Regulations, Part 46, Protection of Human Subjects (revised Nov. 13, 2001). A blood specimen was withdrawn after obtaining written, informed consent from donors. It was mixed immediately with an anticoagulant, and RBCs were pelleted at 800 *g* for 30 min. Then they were resuspended and washed twice with PBS. The suspension was then filtrated through a leukocyte removal filter (Pall, East Hills, NY). The RBC suspensions were prepared at a Hb concentration of 10 g/dl.

The values of the oxygen partial pressure at which Hb is half-saturated and Hill numbers of HbV, Hb solutions, and RBCs were obtained from the oxygen equilibrium curve measured using a Hemox Analyzer (TCS Medical Products, Philadelphia, PA) at 37°C (Table 1). Steady-shear viscosity measurements were performed using a rheometer (Physica MCR 301; Anton Paar, Graz, Austria) at 25°C.

Table 1. *Physicochemical properties of HbV, $Poly_BHb$, Hb, and RBC*

	HbV	$Poly_BHb$	Hb	RBC
[Hb], g/dl	10	10	10	10
Hb/PLP by mol	1/2.5		1/4	
$k'^{(CO)}_{on}$, 10^5 $M^{-1}\cdot s^{-1}$	2.1[a]	2.7[a]	2.1[a]	0.65[b]
$k'^{(NO)}_{on}$, 10^7 $M^{-1}\cdot s^{-1}$	0.61[a]	2.4[a]	2.4[a]	0.012[b]
$k'^{(O_2)}_{off}$, s^{-1}, in 50 mM $Na_2S_2O_4$	32[d]	119[e]	84[d]	4.4[f]
P_{50}, Torr	25–28	54	26	27
Size	279 nm	87–502 kDa[c]	65 kDa	8 μm
Viscosity, mPa·s, at 10^3 s^{-1}	3.75	1.48	1.35	2.46
Viscosity, mPa·s, at 10 s^{-1}	6.88	1.54	1.35	3.18
Perfusion pressure, kPa	21.0–23.0	7.0–8.0	6.0–7.0	9.0–10.0

HbV, Hb-vesicles; $Poly_BHb$, polymerized bovine Hb solution; RBC, red blood cells; [Hb], Hb concentration; PLP, pyridoxal 5′-phosphate; $k'^{(NO)}_{on}$, apparent NO-binding rate constant; $k'^{(CO)}_{on}$, apparent CO-binding rate constant; $k'^{(O_2)}_{off}$, apparent O_2-releasing rate constant; P_{50}, oxygen partial pressure at which Hb is half-saturated. [a]See Ref. 36; [b]see Ref. 4; [c]see Ref. 2; [d]see Ref. 42; [e]measured using a stopped-flow rapid scan spectrophotometer (RSP-1000; Unisoku, Osaka, Japan) by rapidly mixing the $Poly_BHb$ solution (10 μM in PBS) and a 50 mM NaS_2O_4 solution in PBS; [f]see Ref. 52.

Perfusion of Hb-containing Fluids Through Narrow Tubes

Narrow, gas-permeable tubes (25-μm inner diameter; 37.5-μm wall thickness; 150-mm length) were made of a fluorinated ethylene-propylene copolymer (Hirakawa Hewtech, Ibaraki, Japan), as described in previous reports (15, 35, 39, 48) (Fig. 1). One end of the narrow tube was connected to a reservoir of the Hb-containing suspension. The narrow tube was immersed in a water bath (12 cm long × 3 cm width, 0.3 mm depth) made by two acrylic plates with a rubber supporting plate in between, and it was placed horizontally on the stage of an inverted microscope (IX-71; Olympus, Tokyo, Japan). The suspension in the reservoir was mixed gently and continuously with a magnetic stirrer (CC 301; AS One, Tokyo, Japan) and pressurized using a syringe connected to a syringe pump (FP-W-100; Toyo Sangyo, Tokyo, Japan). The perfusion pressure was monitored using a digital pressure sensor (AP-C30; Keyence, Tokyo, Japan). The centerline flow velocity was analyzed using photodiodes and the cross-correlation technique (Velocity Tracker Mod-102 B; Vista Electronics, Ramona, CA) (13). This method usually requires a significant change of contrasts because of the RBCs passing. However, stroma-free Hb (SFHb), $Poly_BHb$, and HbV are distributed homogeneously in the tube; no change of contrast is obtainable. Therefore, we added a small amount of RBCs (5 vol%) to enable centerline velocity measurements. This level of addition would not influence the reaction rate of the whole solution, because we confirmed that perfusion of saline with 5 vol% RBCs (without Hb or HbV) provided negligibly small light absorption spectrum. The centerline velocity was adjusted to 1 mm/s by changing the pressure that was applied to the reservoir. We selected the velocity 1 mm/s in the tube and the gas concentrations (see below) to obtain the absorption changes in the tube of 12 cm length, according to our laboratory's previous paper (39) and a reference paper of Tateishi et al. (48). The water bath was filled with saline containing 10 mM sodium hydrosulfite ($Na_2S_2O_4$; Wako Pure Chemical Industries, Tokyo, Japan), bubbled with pure N_2, low-concentration NO (NO, 4.7%; N_2, 95.3%), or CO (CO, 14.14%; N_2, 85.86%). $Na_2S_2O_4$ is effective to eliminate trace amount of remaining oxygen that might affect the reactions of Hb and CO or NO. The wall of the narrow tube is made of perfluorinated polymer and is permeable only for gas molecules, not for $Na_2S_2O_4$. The entire perfusion experiment was performed at 25°C. In our experiment, the inner volume of the narrow tube is 5.9×10^{-5} cm^3, which is much smaller (1/180,000) than that of the exterior water bath (11 cm^3). We assumed that O_2 is quenched rapidly at the exterior surface of the tube in the O_2-releasing

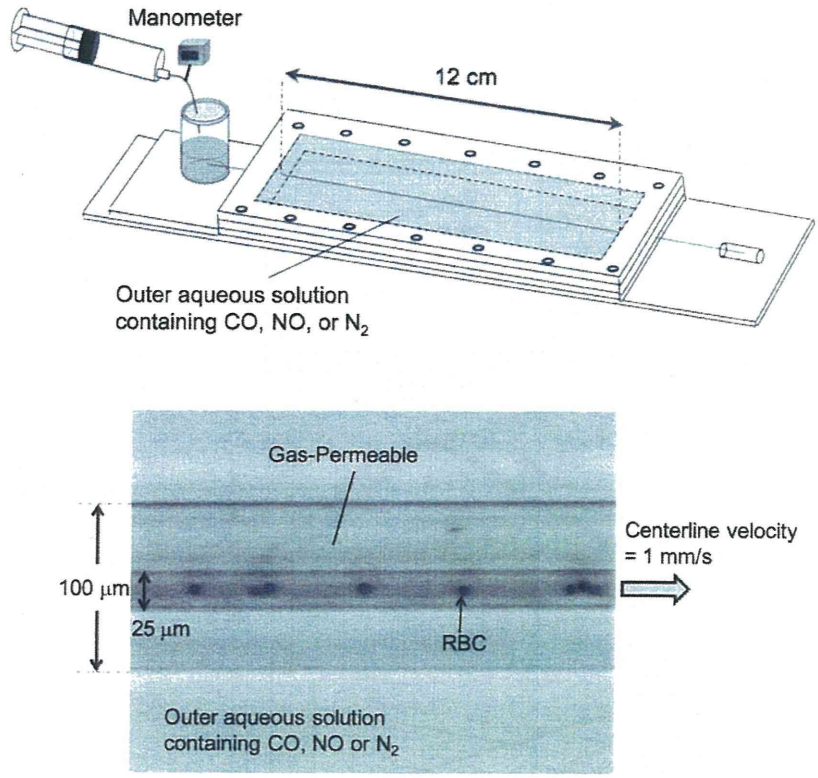

Fig. 1. *Top*: experimental setup of a gas-permeable artificial narrow tube immersed in a water bath made by the gap between two transparent acrylic plates with a rubber supporting plate. One end of the narrow tube was connected to a reservoir of the Hb-containing suspension. The reservoir is pressurized by N_2 gas for perfusion of a fluid through the tube. *Bottom*: microscopic view of a gas-permeable artificial narrow tube. The tube, made of perfluoro polymer, is gas permeable. The tube is immersed in water equilibrated with N_2, low-concentration carbon monoxide (CO), or nitric oxide (NO) gases. The wall thickness, $(100 - 25)/2 = 37.5$ μm, is important, not only for regulation of measurable gas permeability, but also for the stiffness of the tube of greater than 12 cm traveling distance. The centerline flow velocity was adjusted to 1 mm/s. To monitor the velocity, a small amount of red blood cell (RBC) solution is mixed. Measurements of absorption spectrophotometry of the fluid in the tube were performed at several traveling distances.

experiment, and CO and NO are abundant in the exterior area and provided continuously into the tube in the CO- and NO-binding experiments.

Equipment to Monitor Gas Reactions in Narrow Tubes

The apparatus consisted of an inverted microscope with an objective lens of ×40 magnification (ULWD CDPlan 40PL; Olympus), a spectrophotometer (Photonic multichannel analyzer, model PMA-11; Hamamatsu Photonics K.K., Hamamatsu, Japan) connected through a C-mount, a thin optical guide, and a computer (FMV BIBLIO MG50R; Fujitsu, Tokyo, Japan). The microscope's light source (a halogen lamp) intensity was controlled using a current stabilizer (TH4–100; Olympus). The scanned wavelength was 194–956 nm with a gate time of 100 ms/scan; data were obtained every 0.2 nm. One spectrum from a 25-μm-diameter spot over the centerline of the narrow tube was recorded, and 100 scans were accumulated in 10 s. A measuring spot on the narrow tube within the visual field of the microscope was fixed on a monitor (PVM-14L2; Sony, Tokyo, Japan) through a charge-coupled device camera (model CS 230B; Olympus) by sliding the microscope stage.

Measurement of O_2-releasing Rates of Oxygenated Hb-containing Solutions

To measure the O_2 releasing rate, the gas-permeable tube was immersed in deoxygenated saline solution containing 10 mM $Na_2S_2O_4$. The spectroscopic measurements were performed at traveling distances of 10, 30, 50, 70, and 90 mm. After a steady flow was attained, three measurements were performed. Because of the light scatter by fine particles, the absorbance of the HbVs at a shorter wavelength was slightly higher than that at a longer wavelength (41). In the spectra of the 100% deoxy-Hb and 100% oxygenated Hb-containing samples, two isosbestic points (522 and 586 nm) in the Q band of Hb were connected by a straight line as the baseline (Fig. 2*A*). The absorbances at 555 nm [A_{555}; maximum absorbance (λ_{max}) of deoxy-Hb] and 576 nm (A_{576}, λ_{max} of oxyHb) from the baseline were obtained to produce a calibration line that shows the relation between the O_2 saturation (in %) and the ratio of the two absorbances ($R = A_{555}/A_{576}$) (39). The O_2 saturation values of each sample were averaged and shown vs. the traveling distance ($n = 3$, mean ± SD).

Measurement of CO-binding Rate of Deoxy-Hb-containing Solutions

To measure the CO-binding rate, the tube was immersed in a saline solution containing 10 mM $Na_2S_2O_4$, which had been previously bubbled with a gas of 14.14% CO/N_2 balance (Takachiho Chemical Industrial, Tokyo, Japan). The resultant CO concentration outside of the tube was ~135 μM. The spectroscopic measurements were performed by the same manner. In the spectra of the 100% deoxy-Hb and 100% carbonylated Hb-containing samples, two isosbestic points (454 and 578 nm) were connected by a straight line as the baseline (Fig. 2*B*). The A_{555} (λ_{max} of deoxy-Hb) and A_{569} (λ_{max} of HbCO) from the baseline were obtained to make a calibration line that shows the relation between the CO saturation (in %) and the ratio of the two absorbances ($R = A_{555}/A_{569}$). The CO saturation values of each sample were averaged and shown vs. the traveling distance ($n = 3$, mean ± SD).

Measurement of NO-binding Rate of Deoxy-Hb-containing Solutions

The method to measure the NO-binding rate is essentially identical with that of CO-binding rate. A gas of 4.7% NO/N_2 balance (Takachiho Chemical Industrial) was used to attain the NO concentration, ~88 μM. Two isosbestic points (449 and 592 nm) of HbNO and deoxy-Hb were obtained (Fig. 2*C*). The A_{555} (λ_{max} of deoxy-Hb) and A_{575} (λ_{max} of HbNO) from the baseline were used to obtain the calibration curve of NO saturation (in %) vs. $R = A_{555}/A_{575}$.

Simulation of Diffusion Profiles of Hb and HbV in Narrow Tubes

The diffusion and distribution of Hb (6 nm) and HbV (250 nm) in a fluid flowing through a tube (25-μm diameter) were simulated to clarify the stirring effects of the fluids. The profiles of the diffusion of Hb molecules or HbV particles that were originally present just near the wall of the narrow tube (12.5-μm radius, 10-cm length, 1-mm/s centerline velocity) at the entrance are analyzed. We assumed that the two different solutions had identical physicochemical properties. *Component 1* enters the core, with 0- to 11.5-μm tube radius. Then *component 2* enters the peripheral, with 11.5- to 12.5-μm radius. The simulated diffusion of *component 2* to the center and to the flow direction in two-dimensional imaging of the tube cross section was calculated.

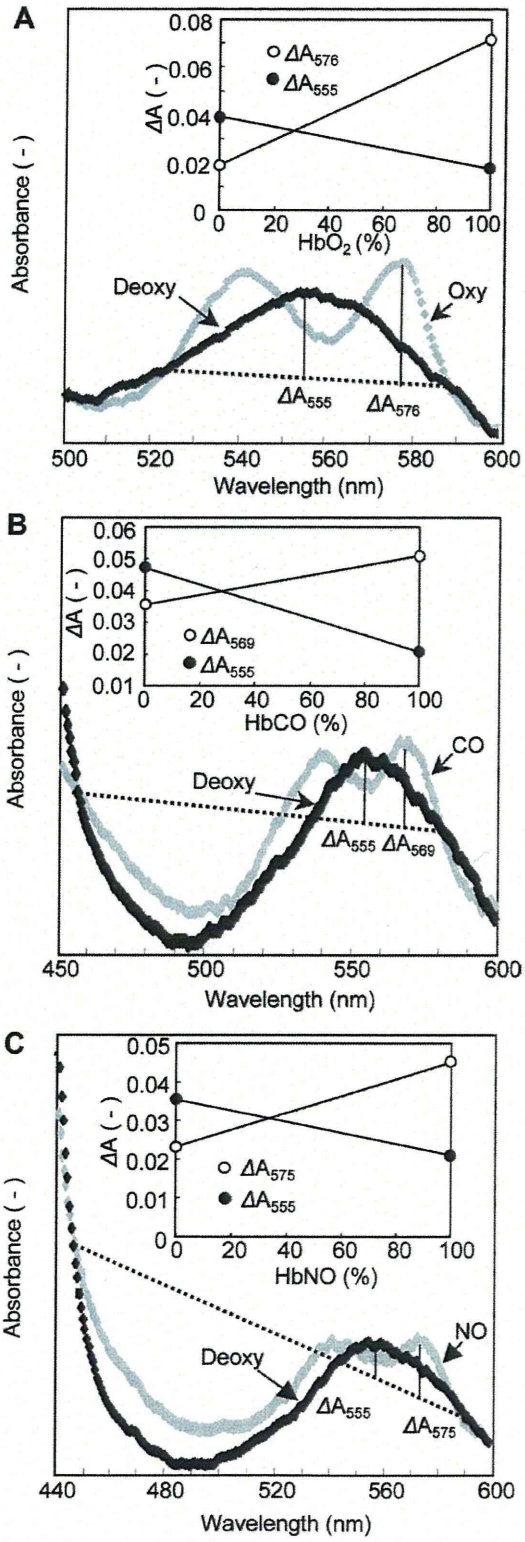

Hb solution. The Hb is much smaller than the tube diameter. The Navier-Stokes equation is solved with the incompressible condition to obtain flow velocity v and pressure p.

$$\rho(\partial v/\partial t) + (\rho v \cdot \nabla)v = -\nabla p + \nabla \cdot \{\eta[\nabla v + (\nabla v)^t]\} \quad (1)$$

where ρ denotes the density, η is the viscosity, and t is time. An advection-diffusion equation is used for solute transport in a flow.

$$\partial C_i/\partial t + \nabla \cdot (-D_i \nabla C_i) = -(v \cdot \nabla)C_i \quad (2)$$

where C_i represents a solute concentration, and D_i is the diffusion constant. The flux density N_i of a solute is expressed as

$$N_i = C_i v - D_i \nabla C_i \quad (3)$$

The tube wall does not allow penetration of the solute; the Neumann condition is adopted as

$$N_i \cdot \mathbf{n} = -D_i \nabla C_i \cdot \mathbf{n} = 0 \quad (4)$$

At the entrance tube, C_i is fixed. At the tube exit, the Neumann condition without the concentration gradient is adopted as $N_i \cdot \mathbf{n} = C_i v \cdot \mathbf{n}$. In fact, D_i is expressed as

$$D_i = kT/(6\pi\eta d_d) \quad (5)$$

where d_d is particle diameter.

HbV suspension. For HbV, the particle size is 1/100 of the tube diameter and is no longer negligible. Actually, HbV is regarded as a solid particle and the fluid as a solid-liquid two-phase flow. A two-phase flow equation is solved for the velocities of the particles and the liquid phase separately, with the assumptions that *1*) the difference in density between HbV and the suspending medium is not large; *2*) the two phases deform and flow together; and *3*) the relative velocity (slip velocity) is determined by the mechanical balance of pressure and slip force.

A mean velocity v and a pressure p is solved by a two-phase flow equation with a slide friction term expressed as *Eq. 6*.

$$\rho(\partial v/\partial t) + (\rho v \cdot \nabla)v = -\nabla p - \nabla \cdot (\rho c_d(1 - c_d)v_{slip}v_{slip}) + \nabla \cdot \{\eta[\nabla v + (\nabla v)^t]\} \quad (6)$$

Therein, ρ signifies the averaged density, c_d is the mass fraction of solid particles, and v_{slip} is the relative velocity between the two phases. For a solid particle dispersion, v_{slip} is expressed as *Eq. 7*.

$$v_{slip} = -[(\rho - \rho_d)d_d^2/(18\rho\eta)]\nabla p \quad (7)$$

Therein, ρ_d the density of solid particles.

Fig. 2. Calculation of reaction levels of oxy-Hb (HbO_2; *A*), HbCO (*B*), and HbNO (*C*) from the absorption changes. *A*: for the oxygen saturation determination, for example, two isosbestic points of the spectra of deoxygenated (deoxy) and oxygenated (oxy) Hb solutions (at 522 and 586 nm) were connected by a straight line (baseline). Based on absorbances at 555 nm [change (Δ) in A_{555}, maximum absorbance (λ_{max}) of deoxy-Hb] and 576 nm (ΔA_{576}, λ_{max} of HbO_2) from the baseline, linear relations between the level of HbO_2 (%) and ΔA_{555} and ΔA_{576} are obtained individually, as shown in the *inset*. Then the ratio of the two absorbances ($R = A_{555}/A_{576}$) was utilized to obtain the level of HbO_2. The levels of HbCO (*B*) and HbNO (*C*) were calculated similarly.

The viscosity η of a multiphase flow depends on the volume fraction of the particles (ϕ) and shear rate (γ) and was obtained by the experimental measurement between the volume fraction and the shear viscosity of the HbV suspension, as shown in *Eq. 8*.

$$\eta(\phi, \gamma) = 0.9\gamma^{-(0.2542\phi + 0.25\phi^2)} e^{4.1278\phi + 4.2207\phi^2} \quad (8)$$

The Maxwell-Stefan advection-diffusion equation was used for a highly concentrated particle dispersion (HbV) to calculate the counter diffusion.

$$\partial \phi_i / \partial t + \nabla \cdot (j_i + \phi_i v) = 0 \quad (9)$$

Therein, j_i is the relative diffusion flux, and ϕ_i is the volume fraction of the component i. The diffusion flux can be expressed by external forces, such as the concentration gradient and pressure, applied to the component i. Therefore, *Eq. 9* is converted as follows with a self-diffusion constant of a solute D_i.

$$\partial \phi_i / \partial t + \nabla \cdot \left[\phi_i v - D_i \left(\nabla \phi_i + \phi_i \frac{\rho - \rho_i}{\rho} \frac{\nabla p}{p} \right) \right] = 0 \quad (10)$$

For calculations, we used the Comsol Multiphysics and Chemical Engineering Module (Comsol, Burlington, MA). Table 2 presents the required physicochemical parameters for simulation.

RESULTS

O_2-releasing Profile

All Hb-containing solutions showed the change of absorption spectroscopy in the Q bands (Fig. 3*A*) as they traveled a longer distance and released oxygen (*lines 2–6*). The two characteristic peaks derived from HbO_2 (*top* lines, 100% HbO_2; λ_{max}, 541 and 576 nm) tended to decrease and a new peak derived from deoxy-Hb (*bottom* lines, 100% deoxy-Hb; λ_{max}, 555 nm) became evident, especially in the case of $Poly_BHb$ and SFHb solutions. Both HbV and RBCs showed two peaks, even at 9-cm traveling distance. Figure 4*A* presents the level of oxygenation vs. the traveling distance of four Hb-containing solutions. At 9-cm traveling distance, both $Poly_BHb$ and Hb solutions released O_2 considerably, and the averaged levels of HbO_2, respectively, became 27 ± 8 and 43 ± 6%. On the other hand, both HbV and RBCs, respectively, remained high levels of HbO_2, 68 ± 7 and 76 ± 4%. The profile of HbV resembled that of RBCs.

Table 2. *Parameters of Hb solution and HbV suspension at [Hb] =10 g/dl for diffusion simulation*

Parameter	
Hb	
Diffusion coefficient*	9×10^{-11} m²/s
Viscosity	1.0 mPa·s
Density of the solution†	1025 kg/m³
[Hb]	10 g/dl, 1.55 mM
HbV	
Volume fraction	0.4
Particle diameter	250 nm
Viscosity of the suspending medium	0.9 mPa·s
Viscosity of the HbV suspension	Data in Table 1
Density of the suspending medium‡	1003.3 kg/m³
Density of HbV particles‡	1067.05 kg/m³

*See Ref. 24. †Measured by a dynamic capillary rheometer (Anton Paar, Graz, Austria). ‡Calculated from the density of the HbV suspension (1028.8 kg/m³), volume fraction (0.4), and the density of the suspending medium (1003.3 kg/m³) as [1028.8 − (1.0 − 0.4) × 1003.3]/0.4 = 1067.05 kg/m³.

CO-binding Profile

Figure 3*B* shows that all of the Hb-containing solutions showed a single peak at 555 nm attributable to deoxy-Hb (*top* lines). The absorption spectrum changes gradually, and two new peaks tended to appear at 540 and 569 nm (*lines 2–6*), indicating the conversion of deoxy-Hb to HbCO (*bottom* lines, 100% HbCO). The HbCO conversion rates of $Poly_BHb$ and Hb solutions were almost identical; the HbCO levels reached 94 ± 3 and 90 ± 3% at 9-cm traveling distance (Fig. 4*B*). On the other hand, HbV showed the lower rate of HbCO conversion, and it reached 71 ± 3% at 9-cm traveling distance, which was almost identical to the profile of RBCs (66 ± 4% at 9-cm traveling distance).

NO-binding Profile

Actually, HbNO has two characteristic peaks at 545 and 575 nm (*bottom* lines in Fig. 3*C*). Both $Poly_BHb$ and Hb solutions tended to show similar spectra of HbNO at 9-cm traveling distance. However, both HbV and RBC showed a slight shoulder at around 575 nm, but the new peaks were not apparent, and the change of the spectrum was not remarkable. Figure 4*C* portrays that the NO-binding profiles of Hb and $Poly_BHb$ solutions were almost identical; they, respectively, reached HbNO levels of 70 ± 5 and 65 ± 5%. They are much faster than the profiles of RBCs (36 ± 3%) and HbV (39 ± 6%).

Simulation of the Diffusion of Hb and HbV in the Narrow Tube

We assumed diffusion of two different fluids with the identical physical property in a tube, namely, HbV-1 as *component 1* and HbV-2 as *component 2*, and simulated how the two fluids are mixed during their flow. Figure 5*A* shows the diffusion of HbV in the narrow tube. The red color signifies that the HbV-2 enters in the peripheral side of the tube (near the wall); the red color gradually turns to yellow, green, and light blue, progressively, with the traveling distance, indicating that the HbV-2 diffuses and is gradually mixed with the HbV-1, and that the HbV-2 concentration decreases. However, the distribution is not homogeneous, even at 100-μm traveling distance. The white lines show trajectory patterns of *component 2*. A particle of 11.5-μm radius located at the entrance diffuses to 9-μm radius from the centerline at 100-μm traveling distance.

The diffusion of Hb is so rapid that the color change is mostly observed only at the entrance in a short traveling distance (<10 μm) (Fig. 5*B*). It becomes homogeneous quite rapidly. The Hb-2 of 11.5-μm radius located at the entrance diffuses to 3-μm radius at 100-μm traveling distance. In fact, Hb reaches the centerline at 1-mm traveling distance. On the other hand, HbV reaches the centerline at 25-mm traveling distance.

DISCUSSION

Our primary finding is that the reactions of NO binding and CO binding and the O_2 release of Hb solutions are markedly retarded for encapsulated Hb (HbV) and RBCs when perfused through artificial narrow plastic tube. These results support the physiological observation that cell-free Hb induces vasoconstriction, but not HbV and RBCs (32).

Conditions of hemolysis (20) and studies related to the development of HBOCs (9, 12, 21, 26, 30, 32, 44, 51) have

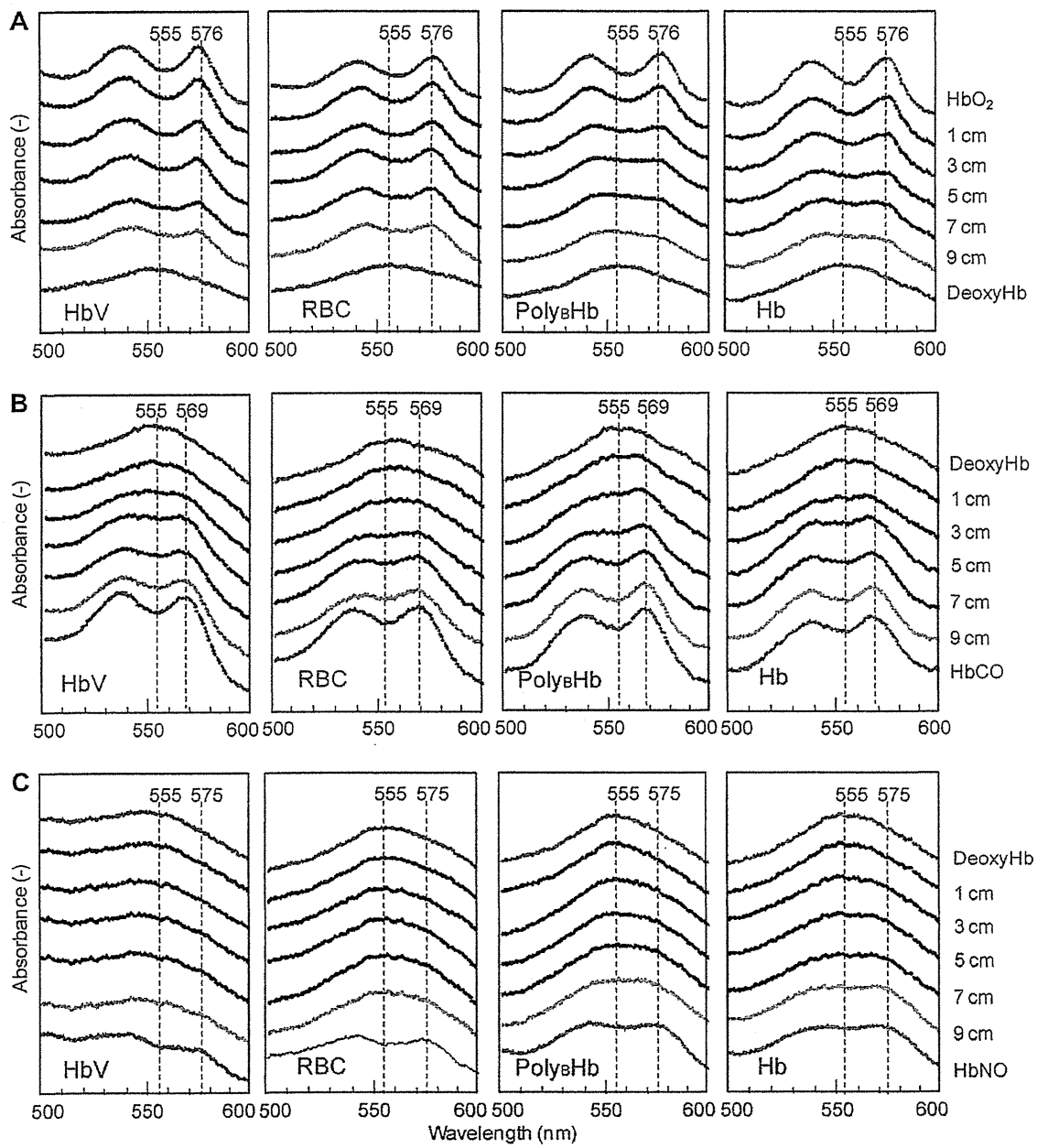

Fig. 3. Spectroscopic changes in Q bands of the Hb-containing fluids by perfusing through the narrow tube at the traveling distances of 1–9 cm. The *top* and *bottom* lines represent the absorption spectroscopy of 0% and 100% reactions, respectively. *A*: measurement of O_2-releasing behavior by perfusing through the narrow tube immersed in an anerobic condition. Two characteristic peaks (λ_{max} = 541 and 576 nm) attributed to HbO_2 decreased with the traveling distance. A new peak (555 nm) attributed to deoxy-Hb increased. *B*: spectroscopic changes in Q bands of the Hb-containing fluids with NO binding perfused through the narrow tube. Two characteristic new peaks attributed to HbNO (λ_{max} = 545 and 575 nm) increased with the traveling distance; deoxy-Hb (555 nm) decreased. *C*: spectroscopic changes in Q bands of the Hb-containing fluids with CO binding perfused through the narrow tube. Two new characteristic peaks attributed to HbCO (λ_{max} = 540 and 569 nm) increased with the traveling distance; deoxy-Hb (555 nm) decreased. PolyBHb, polymerized bovine Hb solution.

shown that the entrapment of endothelium-derived NO induces vasoconstriction, hypertension, reduced blood flow, and vascular damage. Physiological doses of CO are a vasorelaxation factor, especially in the hepatic microcirculation (46). Its entrapment by cell-free Hb solutions induces constriction of sinusoidal capillaries (8). These side effects caused by the presence of molecular Hb in plasma suggest that the cellular structure of RBCs plays a role in ensuring the bioavailability of NO and CO. It has been suggested that faster O_2 unloading from the HBOCs is advantageous for tissue oxygenation (27). However, this concept is controversial in light of recent findings, because an excess O_2 supply would cause autoregulatory vasoconstriction and microcirculatory disorders (31).

The presence of a plasma layer (RBC-free layer) can constitute a diffusion barrier of gas molecules between the vascular wall and RBCs. This explanation is plausible because a